ANTIBIOTIC-BASED STRATEGIES TO OVERCOME DRUG RESISTANCE IN CANCER CELLS THROUGH OXPHOS

by
EDA KAPAN

Submitted to the Graduate School of Engineering
and Natural Sciences in partial fulfillment of
the requirements for the degree of Master of Science

Sabancı University
December 2024

ABSTRACT

ANTIBIOTIC-BASED STRATEGIES TO OVERCOME DRUG RESISTANCE IN CANCER CELLS THROUGH OXPHOS

EDA KAPAN

MOLECULAR BIOLOGY, GENETICS AND BIOENGINEERING M.Sc. THESIS, DECEMBER 2024

Thesis Supervisor: Prof. Dr. Alex Lyakhovich

Keywords: Cancer chemoresistance, Oxidative phosphorylation, Triple-negative breast cancer, Mitochondrial dysfunction, Antibiotic repurposing, Targeted therapy

Chemoresistance represents a significant barrier to effective treatment outcomes in TNBC, making it one of the most difficult subtypes of breast cancer to treat. Conducting *in vitro* and *in vivo* experiments, this study investigated the effectiveness of antibiotics and TPP-conjugated derivatives in inhibiting OXPHOS using cyclophosphamide-resistant MDA-MB-468 TNBC cells and their parental counterparts. The results showed that resistant cells were more sensitive to AMX and FSS antimicrobials, had higher ATP levels, improved mitochondrial function, and higher oxygen consumption. Particularly in resistant cells, AMX treatment successfully reduced MMP-9 and MMP-2 activities as well as the stemness markers Sox-2 and Nanog. TPP-linked antibiotics showed improved efficacy against resistant cells, suggesting effective mitochondrial targeting. Also, combinatorial therapy demonstrated a synergistic effect of cyclophosphamide and AMX in combating resistant cells. Although AMX had little effect on the parent tumors, it dramatically reduced tumor growth in resistant TNBC xenografts, according to *in vivo* studies. In conclusion, antibiotics and their TPP-conjugated derivatives appear to be promising therapeutic approaches to treating chemoresistant TNBC by targeting OXPHOS through various mechanisms including impairing mitochondrial function, reducing stemness, and preventing metastasis.

ÖZET

KANSER HÜCRELERİNDE İLAÇ DİRENCİNİ OKSİDATİF FOSFORİLASYON ARACILIĞIYLA AŞMAK İÇİN ANTİBİYOTİK BAZLI STRATEJİLER

EDA KAPAN

MOLEKÜLER BİYOLOJİ, GENETİK VE BİYOMÜHENDİSLİK
YÜKSEK LİSANS TEZİ, ARALIK 2024

Tez Danışmanı: Prof. Dr. Alex Lyakhovich

Anahtar Kelimeler: Kanser kemoterapi direnci, Oksidatif fosforilasyon, Üçlü negatif meme kanseri, Mitokondriyal disfonksiyon, Antibiyotik yeniden kullanımı, Hedefli terapi

Kemorezistans, TNBC'de etkili tedavi sonuçlarına karşı önemli bir engel teşkil eder ve bu da onu tedavi edilmesi en zor meme kanseri alt tiplerinden biri yapar. İn vitro ve in vivo deneyler yürütülen bu çalışmada, siklofosfamid dirençli MDA-MB-468 TNBC hücreleri ve bunların ayrıca ana hücrelerini kullanarak OXPHOS'u inhibe etmede antibiyotiklerin ve TPP-bağlı antibiyotiklerin etkinliği araştırıldı. Sonuçlar, dirençli hücrelerin AMX ve FSS antimikrobiklere karşı daha duyarlı olduğunu, daha yüksek ATP seviyelerine sahip olduğunu, mitokondriyal işlevlerinin artmış olduğunu ve daha yüksek oksijen tüketimine sahip olduğunu gösterdi. Özellikle dirençli hücrelerde, AMX tedavisi MMP-9 ve MMP-2 enzimlerinin aktivitelerini ve kök hücre belirteçleri Sox-2 ve Nanog'un mRNA ekspresiyonunu başarıyla azalttı. TPP- bağlı antibiyotikler, dirençli hücrelere karşı gelişmiş etkinlik gösterdi ve bu da onların etkili bir şekilde mitokondriyayı hedeflediğini gösterdi. Ayrıca, kombinasyonel terapi siklofosfamid ve AMX'in dirençli hücrelerle mücadelede beraber sinerjik bir etkiye sahip olduğunu gösterdi. AMX'in ana tümörler üzerinde çok az etkisi olmasına rağmen, in vivo çalışmalara göre dirençli TNBC ksenograftlarında tümör büyümesini önemli ölçüde azalttı. Sonuç olarak, antibiyotikler ve TPP-bağlı antibiyotikler mitokondriyal işlevi bozma, kök hücreliği azaltma ve metastazı önleme dahil olmak üzere çeşitli mekanizmalar yoluyla OXPHOS'u hedef alarak kemoterapiye dirençli TNBC'yi tedavi etmek için umut verici terapötik yaklaşımlar sunuyor.

ACKNOWLEDGEMENTS

First and foremost, I want to express my gratitude to my thesis advisor, Assoc. Prof. This has been an inspiring experience for me because of Dr. Alex Lyakhovich's leadership and enthusiasm in this field. Above all, I am grateful for the chance to work in his lab. I want to express my sincere gratitude to him, without whom this would not have been possible. Throughout this thesis project, he consistently offered support and was always eager to help in any way he could. He added interest and ease to the process of finishing my thesis. His generosity and encouragement are greatly appreciated.

Moreover, I would also like to thank all of the members of our laboratory, Cemile USLU and Esra AKKUŞ.

Finally, I would like to sincerely thank my family for their unwavering love, support, and companionship over the years. I want to thank my three older sisters in particular for their constant support and presence during this journey. I am also immensely grateful to my boyfriend, who has supported me through tough times, given me encouragement, and made me feel loved and appreciated.

To my beloved family

TABLE OF CONTENTS

LIST OF FIGURES AND TABLES

LIST OF ABBREVIATIONS

3-MA: 3-Methyladenine

468-Par: MDA-MB-468 parental cells

468-Rcyclo: MDA-MB-468 cyclophosphamide-resistant cells

ADP: Adenosine diphosphate

AMX: Amoxicillin sodium

AP-1: activating protein-1

APS: Ammonium persulfate

ATP: Adenosine triphosphate

Bac: Bacitracin

BCA: Bicinchoninic acid

BSA: Bovine serum albumin

CDK4/6: Cyclin-dependent kinase 4/6

cDNA: Complementary DNA

CSC: Cancer stem cells

Cyclo: Cyclophosphamide

DMEM: Dulbecco's Modified Eagle Medium

DMSO: Dimethyl sulfoxide

DNAse: Deoxyribonuclease

dNTP: Deoxynucleoside triphosphate

DXR: 1-deoxy-D-xylulose 5-phosphate reductoisomerase

ECM: Extracellular membrane

EDTA: Ethylenediaminetetraacetic acid

EMT: Epithelial-mesenchymal transition

ETC: Electron transport chain

FCCP: Carbonyl cyanide-4 (trifluoromethoxy) phenylhydrazone

FLT3: Fms-like tyrosine kinase 3

FSS: Fosmidomycin sodium salt

HIF-1α: Hypoxia Inducible Factor 1 Subunit Alpha

IC[X]: Inhibitory concentration required to inhibit the activity by [X]%

ITD: Internal tandem duplication

JC-1: Iodide salt

MCL1: Induced myeloid leukemia cell differentiation protein

MDF: Mitochondrial dysfunction

MEP Pathway: Methylerythritol phosphate pathway

MMP: Matric metalloproteinases

mtDNA: Mitochondrial DNA

MTT Assay: 3-[4,5-dimethylthiazol-2-yl]-2,5 diphenyl tetrazolium bromide assay

NADH: Oxidized nicotinamide-adenine dinucleotide

Nanog: Nanog homeobox

NF-κB: Nuclear Factor kappa B

OCR: Oxygen consumption rate

OXPHOS: Oxidative phosphorylation

PBS: Phosphate-buffered saline

PCR: Polymerase chain reaction

PVDF: polyvinylidene difluoride

RIPA Buffer: Radioimmunoprecipitation assay buffer

RNAse: Ribonuclease

SDS: Sodium dodecyl sulphate

Sox-2: SRY-box transcription factor 2

STAT-3: Signal transducer and activator of transcription 3

TCA cycle: The citric acid cycle

TEMED: N,N,N′,N′ -Tetramethylethylenediamine

TNBC: Triple-negative breast cancer

TPBS: Tris phosphate-buffered saline

TPP: Triphenylphosphonium

1. INTRODUCTION

In the 21st century, cancer is a significant social, public health, and economic issue that accounts for nearly one in six deaths (16.8%) overall and one in four deaths (22.8%) from noncommunicable diseases (NCDs) globally (Bray et al., 2024). In 177 out of 183 countries, cancer is one of the top three causes of death for people aged 30 -69 years. In this age group, it also accounts for 30.3% of the premature deaths worldwide from NCDs (Bray et al., 2021). Even with the tremendous efforts made in the areas of cancer research, prevention, detection, and treatment, cancer remains one of the world's leading causes of death (Kumar & Jaitak, 2019). Nearly 20 million new cases and 9.7 million cancer-related deaths occurred globally in 2022 (*Cancer Statistics - NCI*, 2024).

According to the approximated new cases in 2024, the major common cancers in the order of decreasing number of cases are as follows: “Breast cancer, prostate cancer, lung and bronchus cancer, colon and rectum cancer, melanoma of the skin, bladder cancer, kidney and renal pelvis cancer, non-Hodgkin lymphoma, endometrial cancer, pancreatic cancer, leukemia, thyroid cancer, and liver cancer.” (*Cancer Statistics - NCI*, 2024). 666,000 deaths from female breast cancer (6.9% of all cancer deaths) make it the fourth most common cause of cancer mortality globally (Bray et al., 2024). The most aggressive type of breast cancer is known as triple-negative breast cancer (TNBC), which makes up 15–25% of all cases of breast cancer and is recurrent by nature (Almansour, 2022).

Cancers are tumors derived from epithelial cells that divide uncontrollably and immortally, in contrast to normal cells. These tumors may be malignant or benign, with the latter having the capacity to spread to other parts of the body by invading neighboring tissues. Malignant tumors are typically biologically complex and show significant spatial variation in histopathology, biochemistry, gene expression, and macroscopic structure (Vamvakas et al., 2020). Depending on which organ or tissue of the human body is impacted, there are more than 100 distinct forms of malignancies.

1.1 Triple-Negative Breast Cancer

Breast cancer is the most prevalent cancer among women worldwide and the second most common type of cancer overall (Parkin et al., 2005). Breast cancer usually begins in the cells of the milk ducts or lobules before spreading to the breast tissue. The uncontrolled proliferation of aberrant cells within the breast, which may invade nearby tissues and potentially spread to other parts of the body, is a hallmark of this disease (Bertos & Park, 2011). The disease is diverse, with multiple subtypes, each exhibiting unique gene expression patterns and overall survival rates (Sørlie et al., 2001). The presence or lack of three receptors—the human epidermal growth factor receptor-2 (HER-2), progesterone receptors (PR), and estrogen receptors (ER)—is typically used to diagnose these subtypes of breast cancer (Johnson et al., 2021). More than 60% of all patients with breast cancer have ER, PR, and HER-2 positive results. Women who do not express ERα, PR, or HER-2 account for about 15% of all cases of breast cancer and are therefore classified as having triple-negative breast cancer (TNBC) (Kurebayashi, 2009).

TNBC patients are insensitive to the majority of currently available hormonal, ER-targeted, and HER-2-based therapies due to their lack of ER, PR, and HER-2. Only conventional chemotherapy is used to treat them, which leaves them vulnerable to a high rate of both systemic and local recurrence (Chen & Russo, 2009). In terms of genes linked to breast cancer susceptibility, TNBC patients have a number of traits in common. Since normal BRCA1 and BRCA2 play a crucial role in DNA repair, over 80% of carriers of BRCA-1 mutations are triple negative, and 20% of patients with breast cancer who have mutations in both BRCA-1 and BRCA-2 also have deficiencies in DNA repair. TNBC patients with such mutations are more vulnerable to DNA-damaging drugs (Fasano & Muggia, 2009). Poor differentiation, high malignancy, increased chance of recurrence, and poor prognosis are characteristics of TNBC. Distant metastases are twice as common in TNBC patients as in women with other breast cancers. TNBC patients thus have a lower survival rate (Cleator et al., 2007).

1.2 Metastasis

Although individual cancer cells have very different genetic and epigenetic characteristics, cancer is frequently referred to as a disease of the genes. Cancer cells

share a number of common traits including the ability to proliferate continuously, the induction of angiogenesis, the evasion of growth suppressors, resistance to cell death, replicative immortality, the ability to invade and spread, the ability to evade immune attack, genomic instability, inflammation, and continuous energy production (Hanahan & Weinberg, 2011a).

Malignant tumor cells are transported from the original neoplasm to a different location by a sequence of distinct biological processes known as tumor metastasis (Steeg, 2006). Since metastasis is the primary cause of death for over 90% of cancer patients, it remains a crucial aspect of cancer malignancy (Steeg, 2006). Cancer cells must leave their primary site, travel through the bloodstream, withstand blood vessel pressure, adapt to new cellular environments in a secondary site, and evade lethal immune cell combat for metastases to develop (Massagué & Obenauf, 2016).

Often, malignant tumor cells undergo the so-called epithelial-mesenchymal transition (EMT) in order to develop a phenotype that enables them to infiltrate both nearby and distant tissues (Tham & Abastado, 2011). Through adherens junctions, tight junctions, and desmosomes, epithelial cells preserve apical-basal polarity and communication with neighboring cells. In contrast, mesenchymal cells lacking the characteristic apical-basolateral polarity of epithelial cells, are separated from one another by the extracellular matrix and lack a basal lamina that separates them from surrounding tissue. Consequently, tumor epithelial cells become mesenchymal cells upon activation of EMT, losing their cell polarity and cell-cell adhesion and acquiring migratory and invasive characteristics (Ribatti et al., 2020).

1.3 Cancer Stem Cells

There have been numerous reports of cellular heterogeneity in a range of solid and hematopoietic malignancies. One notable aspect of cellular heterogeneity is the varying levels of tumor-initiating potential displayed by different cancer cells that coexist inside the same tumor. The term tumor-initiating cells (TICs) or cancer stem cells (CSCs), refers to these more carcinogenic cells because, despite their malignant nature, they are similar to normal stem cells in that they can self-renew and produce more differentiated derivatives (Ye & Weinberg, 2015). The development of primary tumors was promoted and metastasis was accelerated by these stem cell-like characteristics (Ribatti et al., 2020).

In addition to their pluripotency and capacity for self-renewal, CSCs have improved capacities for tumor growth initiation, proliferation, invasion, migration, and resistance to therapies (Batlle & Clevers, 2017). Because of their cell dormancy, improved capacity for DNA damage repair, and improved drug efflux, CSCs are able to withstand oxidative stress or DNA damage when non-CSCs are destroyed by conventional chemotherapy or radiation treatments (Lytle et al., 2018). The following biomarkers of CSCs have been found in breast cancers: ABCG2, ALDH1, CD24, CD44, CD133, SSEA-3, Nectin-4, MUC1, Sox-2, Oct4, and Nanog, Lrg5, and CD70 (X. Zhang et al., 2020). MicroRNAs were also identified as markers of breast CSC subpopulations, controlling the signaling pathways that help breast CSC develop and persist (oncogenic: miR-22, miR155, miR181, and miR221/222 cluster; tumor-suppressive: Let-7, miR34, miR200 family, miR30, and miR600) (Pinto et al., 2013).

1.4 Drug Resistance in Cancer

A significant barrier to cancer treatment and overall patient survival is drug resistance, which is defined as a decline in the ability of anti-cancer drugs to continue their therapeutic effects due to cancer cells becoming resistant to it (Nikolaou et al., 2018). Since the discovery of targeted therapies with several effective chemotherapeutic agents have been approved, however, cancer drug resistance continues to be a major obstacle to their success in addition to being the cause of their potentially fatal side effects (Oun et al., 2018).

There are several distinct models to explain how cancer drug resistance develops. In the conventional model, tumor heterogeneity is explained by clonal evolution theory, whereas the CSC model extended the idea to encompass the hierarchical growth and plasticity of cancer cells (Carvalho et al., 2021). According to the conventional theory of therapy resistance, cells acquire resistance after receiving a specific treatment (Ramos et al., 2021). Drug resistance may develop in a population of tumor cells due to genetic alterations (Hamed et al., 2019). A tumor composed of the clonal offspring of the drug-resistant cells develops after chemotherapy exposure, as only the drug-resistant cells survive and multiply. All of the cancer cells consequently develop drug resistance (O'connor et al., 2014).

The CSC model suggests that most tumor cells are differentiated cells with limited

capacity for replication, while a tiny subset of cancer cells can propel tumor growth and metastasis. Following drug exposure, only the CSCs remain viable due to residing in specialized niches, which are complex microenvironmental structures composed of extracellular matrix proteins, blood vessels, and immune cells that provide essential protection and maintain stemness properties (Plaks et al., 2015). Also, their slow division rate, makes CSCs particularly resistant to conventional cancer treatments which primarily target rapidly dividing cells (Dean et al., 2005). While CSCs typically exist in a dormant state, they possess the remarkable ability to transition between dormancy and activation in response to specific environmental cues (Sosa et al., 2014). Upon activation, these cells demonstrate significant cellular plasticity, enabling them to differentiate into various tumor cell types within their tissue lineage, a process heavily influenced by the surrounding metastatic microenvironment (Batlle & Clevers, 2017). The tumor mass is then subsequently repopulated by these stem cells after they have divided and produced differentiated cells from the stem cells (Napel et al., 2018).

The mechanisms that can enable or promote drug resistance in cancer cells directly or indirectly include drug inactivation, alterations of drug targets, drug efflux (or influx), enhanced DNA damage repair, cell death inhibition, tumor heterogeneity, EMT, cancer stemness, mitochondrial alteration, and oxidative phosphorylation (OXPHOS) (Housman et al., 2014; Mostafavi & Eskandari, 2024) (Figure 1.1). Whether it is chemo-, radio- or immunotherapy, the main cause of resistance patterns to these treatments is genetic mutations that reduce treatment effectiveness through versatile pathways (Holohan et al., 2013). For instance, mutations in DNA repair pathways can simultaneously confer resistance to both chemotherapy and radiotherapy, while alterations in immune checkpoint molecules can affect both conventional and immunotherapeutic approaches (Sharma et al., 2017). This convergence of resistance mechanisms aligns with the principles of evolution, where cancer cells undergo selective pressure during treatment, leading to the survival and proliferation of resistant clones (Greaves & Maley, 2012).

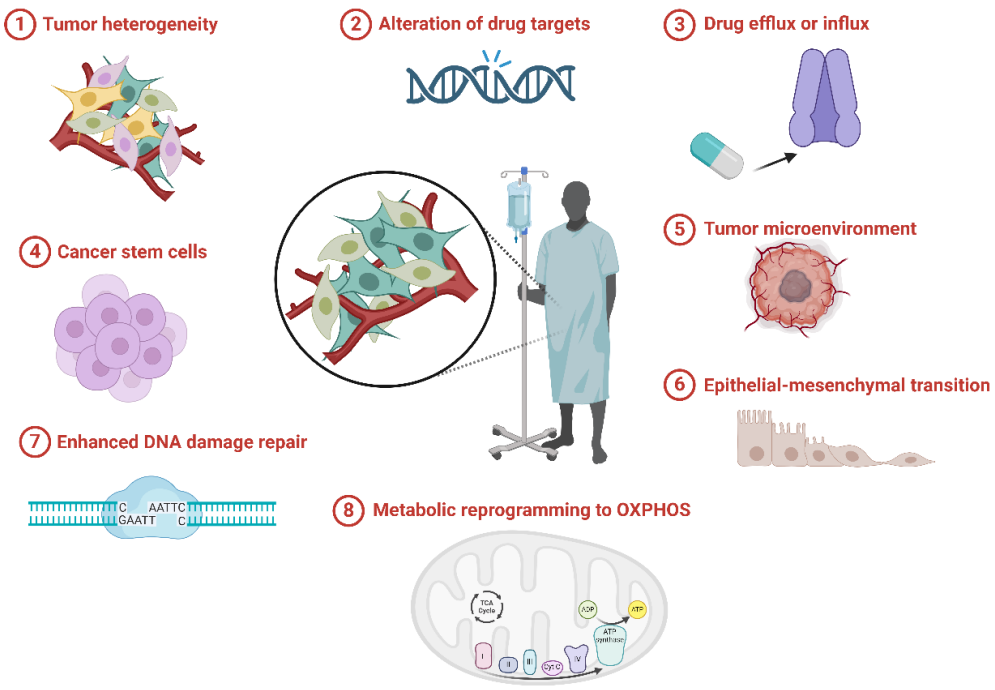

Figure 1.1: Common drug resistance mechanism in cancer treatment.
This figure was created with Biorender.com.

Both the CSC and the conventional models of cancer drug resistance suggest that tumors are heterogeneous. There are temporal and regional differences in stromal architecture, oxygen consumption, glucose metabolism, protein, and growth factor expression as a result of this genetic heterogeneity, which is also continuously vulnerable to different environmental stressors (Ramos et al., 2021). Tumor subregions arise as a result, each exhibiting unique spatial patterns of blood flow, vessel permeability, cell division, cell death, and other characteristics. Because resistant clones persist and multiply, intertumor and intratumor heterogeneity can cause targeted therapies to fail, even with validated targets and medications (Napel et al., 2018).

Multi-drug resistance (MDR) is a particular type of drug resistance in cancer where cancer cells develop cross-resistance to a broad range of structurally and pharmacologically unrelated cancer cytotoxic medications (Kuete & Efferth, 2015). Primarily, ATP binding cassette (ABC) transporter proteins are overexpressed, which effectively effluxes a variety of chemotherapeutic agents outside of cancer cells. This lowers the intracellular drug concentration, making chemotherapy ineffective (Kadioglu et al., 2016). On the other hand, the effectiveness of anticancer medications frequently depends on metabolic activation, but cancer cells can become resistant if the inactivation of these drugs occurs by their mutated drug-metabolizing enzymes (Michael & Doherty, 2005).

One of the most important problems in cancer treatment is the connection between drug resistance and DNA damage response (DDR). Numerous traditional anticancer drugs, such as topoisomerase inhibitors, alkylating agents, and platinum compounds, induce DNA damage to promote cancer cell death (Lord & Ashworth, 2012). However, the therapeutic intent of these medications can be effectively neutralized when cancer cells develop resistance due to improved DNA repair capabilities (O'Connor, 2015). Cell may rescue DNA-damaging agent through enhanced DNA-damage repair response and inactivation of p53, allowing cancer cells to survive and continue proliferating despite treatment (Mountzios et al., 2008).

Moreover, the way certain anticancer medications interact with their respective targets determines how effective they are. Drug resistance, however, may result from changes like target gene mutations and elevated expression levels of target proteins like kinases (Peters et al., 2002). It is also demonstrated that EMT-induced stemness properties contribute to therapy resistance by promoting cellular dormancy and self-renewal capabilities, ultimately leading to treatment failure and disease recurrence (Yang et al., 2014; Zheng et al., 2015). Through their involvement in EMT, matrix metalloproteinases (MMPs), a class of enzymes frequently seen in the breakdown of the extracellular membrane, play a crucial role in the metastasis of cancer (Hanahan & Weinberg, 2011). Overexpression of MMP is indicative of poor prognosis, progression, and metastasis of cancer (Mustafa et al., 2022).

Another process that can change the fate of resistance is autophagy. Autophagy is a catabolic process that has been conserved throughout evolution where cellular components, including damaged organelles and misfolded proteins, are sequestered within double-membrane vesicles called autophagosomes and subsequently degraded through fusion with lysosomes (Mizushima & Komatsu, 2011). In cancer, autophagy plays a context-dependent dual role referred to as the "autophagy paradox". During early tumorigenesis, autophagy acts as a tumor suppressor by maintaining cellular homeostasis, reducing oxidative stress, and preventing the accumulation of damaged cellular components that could promote genomic instability (White, 2012). However, in established tumors, autophagy often serves as a pro-survival mechanism that allows cancer cells to survive under metabolic stress conditions, including nutrient starvation, hypoxia, and chemotherapy-induced damage (Amaravadi et al., 2019; Sun et al., 2011). This survival mechanism is particularly evident in aggressive cancers, where increased autophagy supports tumor growth by recycling cellular components to maintain energy

homeostasis and by promoting resistance to various cancer therapies (Levy et al., 2017). Additionally, inducing autophagy may encourage quiescence and slow cycling, which, when combined with the activation of the hedgehog, Notch, and Wnt self-renewal pathways, results in EMT to avoid the cytotoxic effects of drugs. This, in turn, causes or encourages stem-cell-like characteristics in these cells (Giroux Leprieur et al., 2016; F. Wang et al., 2016). The pro-survival transcription factors AP-1, STAT-3, and NF-κB are also advantageous when constitutively expressed (Bharti & Aggarwal, 2002; Han et al., 2013; Takeuchi et al., 2006).

As previously stated, CSCs exhibit stem-like characteristics, including quiescence, altered metabolism, overexpression of drug efflux transporters, enhanced DNA repair, immune system elusion, self-renewal and differentiation, and more (J. Zhao, 2016). Poor clinical outcomes and chemoresistance in cancer patients are ultimately caused by these characteristics, which facilitate the invasion, metastasis, and relapse of cancer in patients following chemotherapy (Samuel et al., 2020). Biological processes mediated by mitochondria, such as metabolic reprogramming, mitochondrial dynamics, and mtDNA gene adaptation, collectively contribute to the adaptation of cancer cells to treatment. For example, there has been evidence of a significant correlation between drug resistance and the high level of OXPHOS in cancer cells (Mostafavi & Eskandari, 2024). Additionally, mitochondria enhance the adaptability of cancer cells to stressors by reprogramming their quantity, structure, and location (Henkenius et al., 2017; H. Wang et al., 2020). Even though the drug resistance mechanisms are well studied, and several innovative chemotherapy techniques are introduced, the main problem in successful cancer treatment is still chemoresistance.

1.5 Mechanism of Cyclophosphamide Action and Resistance

Almost all of the medications used to treat the most malignant cancers have been found to exhibit resistance to chemotherapy, which is not unexpected considering the complexity and vastness of drug resistance mechanisms in cancer. Cancer treatment protocols are predominantly based on chemotherapy and/or radiotherapy as standard therapeutic approaches, with about 80% of cancer patients receiving chemotherapy during their treatment (DeVita & Chu, 2008). In particular, in the treatment of breast cancer, several chemotherapeutic agents have shown significant effectiveness, including

platinum-based drugs such as cisplatin and carboplatin, and anthracyclines such as doxorubicin, which target rapidly dividing cancer cells through different mechanisms (Perez, 2004; Rayner & Cutts, 2023; Waks & Winer, 2019). In TNBC, cyclophosphamide remains a cornerstone of treatment and is typically administered as part of combination therapies due to its proven effectiveness in targeting DNA synthesis and cell division in aggressive TNBC cells (Garrido-Castro et al., 2019).

However, it has been demonstrated that cyclophosphamide resistance results in cancer recurrence in breast cancer, which is linked to a shorter survival time (Sládek et al., 2002; Stork & Schreffler, 2014). The cancer drug cyclophosphamide is among the oldest which was included in cancer treatment in 1959 after being discovered as early as 1958 (Stork & Schreffler, 2014). In addition to various epithelial tumors like breast, ovarian, and small-cell lung carcinomas, the treatment of hematological malignancies like lymphoma and leukemia continues to rely heavily on cyclophosphamide (Emadi et al., 2009).

It is possible to administer cyclophosphamide intravenously as well as orally. The rate of absorption is extremely high following oral administration. For cytotoxic effects to occur, bio-activation is required (J. Zhang et al., 2005). The oxidation of cyclophosphamide to 4-hydroxy-cyclophosphamide by cytochrome P450, primarily CYP 2B6 and 3A4 (apart from CYP 2A6, 2C8, 2C9, 2C19, and 3A5), results in an equilibrium with aldophosphamide. The substance that can prevent DNA from forming cross-links, phosphoramide mustard, is produced when both forms break down inside the cell. Aldophosphamide cleaves to produce acrolein, which accumulates in the bladder and can be extremely toxic (Ahlmann & Hempel, 2016) (Figure 1.2).

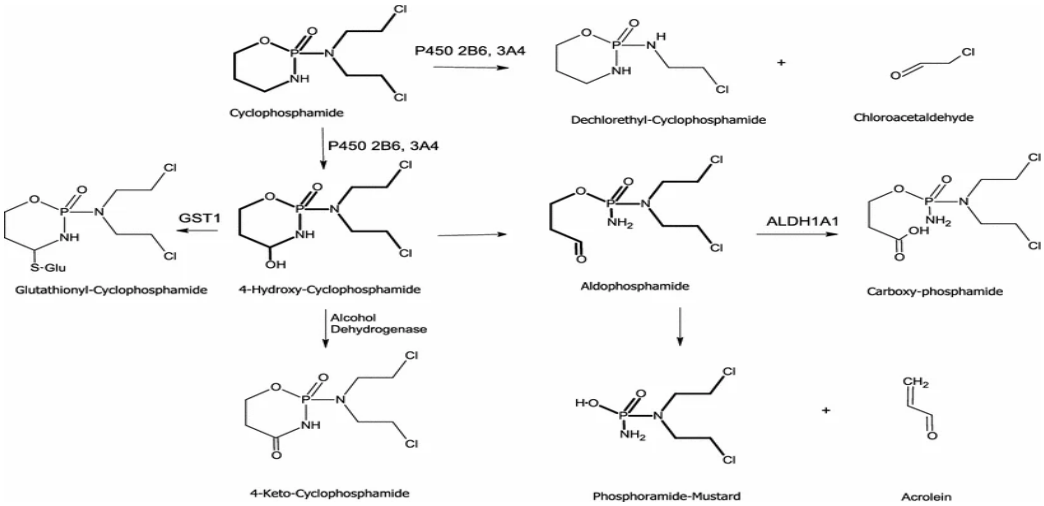

Figure 1.2: The metabolic pathway of cyclophosphamide (Ahlmann & Hempel, 2016).

Cyclophosphamide functions by nonphase-specifically disrupting the cell cycle. The antitumor activity of cyclophosphamide's metabolite, phosphoramide mustard, is responsible for the majority of its effects. The formation of cross-links in DNA at guanine N-7 positions, both between and within DNA strands, is how phosphoramide mustard halts cell division, and consequently, this results in cell death and is irreversible (Stork & Schreffler, 2014). ALDH, or cellular aldehyde dehydrogenase, is the primary detoxification mechanism of cyclophosphamide, particularly ALDH1A1. The active metabolite phosphoramide mustard is prevented from forming by the high expression of ALDH1A1 in rapidly proliferating cells with high carcinogenic potential, such as hematopoietic stem cells, which can withstand higher concentrations of activated cyclophosphamide (Ahlmann & Hempel, 2016; Januchowski et al., 2013). Although it is one of the oldest cancer drugs and is used to treat many types of cancer, there are increasing problems with resistance to cyclophosphamide in chemotherapy patients. This resistance is thought to be related to the increased OXPHOS dependence of cancer cells and CSCs. A study showed that TNBC cells resistant to cyclophosphamide, cisplatin, and doxorubicin exhibited increased mitochondrial activity, as illustrated by the upregulated expression of mitochondrial proteins involved in the TCA cycle and mitochondrial complexes I and V (Abad et al., 2019).

1.6 Role of OXPHOS in Chemoresistance

Otto Warburg discovered in 1924 that even in the presence of oxygen, cancer cells enhanced their uptake of glucose and increased their glycolysis to increase adenosine triphosphate (ATP) production. This phenomenon has been called the Warburg effect, suggesting that malignant tumors are susceptible to glycolysis (Warburg, 1956). In recent years, however, several researchers discovered that after receiving anticancer medication, cancer cells exhibit increased OXPHOS activity with functional mitochondria (Z. Zhao et al., 2023). In contrast to drug-resistant cancer cells, which have reprogrammed metabolisms that cause a shift toward OXPHOS through the expression of specific oncogenes, drug-sensitive cancer cells increase glucose usage and undergo enhanced glycolysis (M. Lee et al., 2019).

OXPHOS is the final stage of cellular respiration that involves a series of redox reactions where electrons flow through membrane-bound proteins to generate ATP (Figure 1.3).

OXPHOS system is found in the inner membrane of the mitochondria and uses the electron transport chain (ETC), which is made up of Complexes I–V and the electron carriers coenzyme Q (CoQ) and cytochrome c (CytC) (Z. Zhao et al., 2023). Complex I receives electrons from NADH at the start of the process and routes them to CoQ. After passing through Complex III and CytC, electrons are transferred to Complex IV, which produces water through oxygen reduction (Zong et al., 2016). By pumping H+ ions into the intermembrane space, Complexes I, III, and IV create a proton gradient during this process, which Complex V uses to produce ATP (Z. Zhao et al., 2023).

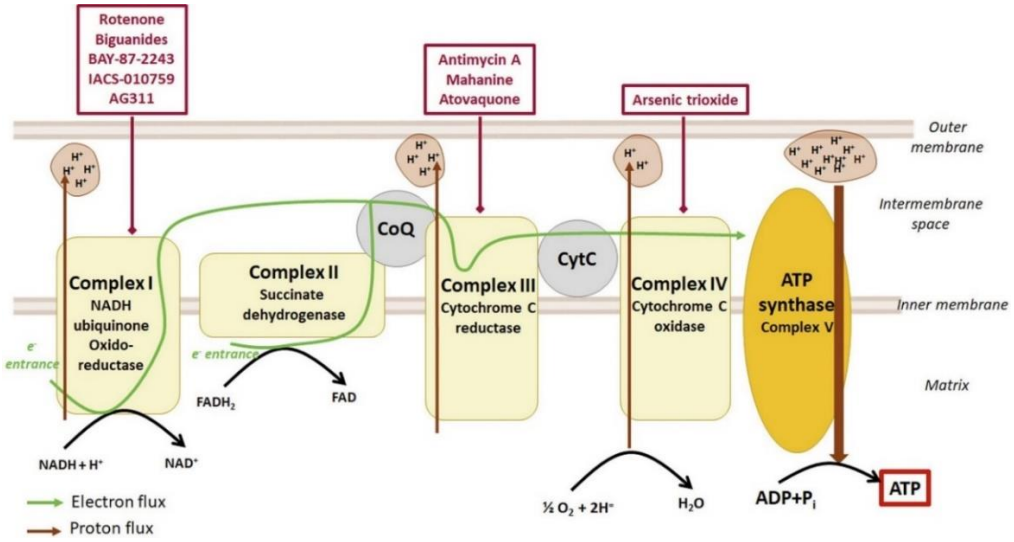

Figure 1.3: Main components of the mitochondrial OXPHOS system and some of their corresponding inhibitors (Cadassou & Jordheim, 2023).

Several studies including ours show that OXPHOS is upregulated in various cancers and contributes highly to chemotherapy resistance (Uslu et al., 2024). Chemoresistant stem-like cells in Ras-driven pancreatic ductal adenocarcinoma (PDAC) exhibited reduced glycolysis and a strong dependence on OXPHOS, according to transcriptome and metabolic analyses (Viale et al., 2014). FLT3 inhibitor gilteritinib is used as a frontline treatment for acute myeloid leukemia (AML) patients, however, *FLT3*- ITD AML cells have been shown to develop resistance to gilteritinib by switching from glycolysis to OXPHOS (P. Zhang et al., 2022). In triple-negative breast cancer (TNBC), breast CSCs (BCSCs) can withstand cytotoxic chemotherapy by overexpressing MYC and MCL1. To encourage CSC enrichment, MYC, and MCL1 increase OXPHOS activity, which in turn raises HIF-1α expression (K. M. Lee et al., 2017). Because drug-resistant cancer cells have higher levels of OXPHOS, OXPHOS inhibitors have the potential to eradicate these cells (Ashton et al., 2018).

1.7 Targeting OXPHOS to Overcome Cancer Resistance

Various OXPHOS inhibitors were suggested to disrupt the main energy mechanism of the drug-resistance cancer cells (Figure 1.4). A few of the different OXPHOS inhibitors, including atovaquone, mahanine, and metformin, show how focusing on the mitochondrial complexes can successfully interfere with the metabolism of cancer cells and overcome drug resistance. In MCF-7 breast cancer cells and CSCs, atovaquone functions as a mitochondrial complex III inhibitor to interfere with the OXPHOS system, lowering the oxygen consumption rate (OCR) and reducing tumor hypoxia at pharmacologically attainable concentrations (Fiorillo et al., 2016). Both mahanine and antimycin A, complex III inhibitors, showed promise in treating drug resistance and relapse in lung cancer patients by specifically targeting lung cancer stem cells and their renewal through downregulating the Wnt/β-catenin pathway, which is involved in stemness (Yeh et al., 2013). Furthermore, the resistance of TNBC cells to the CDK4/6 inhibitor palbociclib is delayed by the complex I inhibitor IACS-010759 (Evans et al., 2021). A new way in the treatment of TNBC is found to be the use of metformin, a biguanide that inhibits complex I, to downregulate RAD51 expression and overcome cisplatin resistance (Samuel et al., 2020).

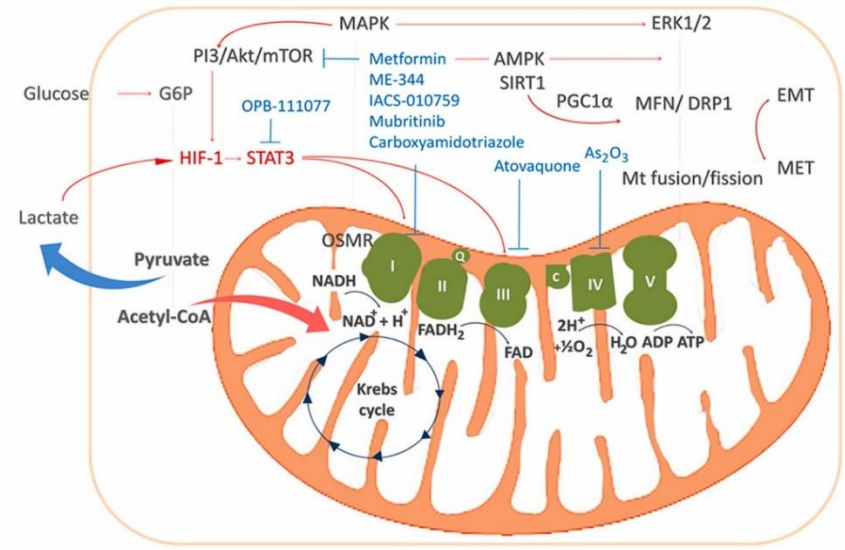

Figure 1.4: Possible targets of OXPHOS inhibitors (Uslu et al., 2024).

Antibacterial drugs (antibiotics) are emerging as a promising drug class for cancer treatment due to their ability to selectively disrupt mitochondrial function, a hallmark of many cancer cells that rely on OXPHOS for ATP production and growth (Machado et al.,

2023). The intriguing evolutionary history of mitochondria and the endosymbiotic theory provide the best explanation for their use. The well-recognized Endosymbiotic Theory of Evolution (Margulis & Bermudes, 1985) states that mitochondria originated from α-proteobacteria that formed a symbiotic relationship with the precursors of eukaryotic cells to avoid growing environmental threats. The structure of bacterial and mitochondrial ribosomes is similar. Several characteristics, such as the mitochondria's double-membrane structure, their DNA, and—most importantly—their machinery for protein synthesis, which is very similar to that of bacteria, demonstrate this bacterial origin (Akhunzianov et al., 2023). Also, nearly 48 proteins make up the 39S large mitoribosomal subunit, the majority of which are homologs of bacterial ribosomal proteins (Koc et al., 2001). Because of this, mitochondria might be especially vulnerable to antibiotic mechanisms that affect transport pathways, protein synthesis, and nucleic acid synthesis (Miller & Singer, 2022). Moreover, mitochondria resemble gram-negative bacteria due to their evolutionary origin as endosymbiotic prokaryotes. Like gram-negative bacteria, mitochondria have a double membrane, with an outer membrane and an inner membrane that encloses the matrix (Gray, 2012). Therefore, antibiotics that are effective on gram-negative bacteria may also be effective on mitochondria.

This bacterial heritage suggests a unique therapeutic opportunity: since mitochondrial ribosomes and bacterial ribosomes have structural similarities, some antibiotics that target bacterial protein synthesis can also affect mitochondrial function (Akhunzianov et al., 2023). Numerous studies have shown how effective antibiotics are on mitochondria. Tetracycline derivatives, for example, have been shown to specifically target mitochondrial translation in cancer cells, resulting in reduced OXPHOS activity and cell death (Lamb et al., 2015). Another study demonstrated the therapeutic potential of tigecycline by showing that it selectively killed leukemia stem cells while sparing normal hematopoietic cells by targeting mitochondrial translation (Škrtić et al., 2011).

Some antibiotics that target protein synthesis in gram-negative bacteria include Amoxicillin sodium (AMX), Fosmidomycin sodium salt (FSS), and bacitracin. AMX, a member of the β-lactam family, inhibits the synthesis of cell walls by attaching itself to penicillin-binding proteins in the cell wall and ultimately causing lysis of the corresponding cell. It can be used for both gram-positive and gram-negative bacteria (Kaur et al., 2023). FSS is an antibiotic notable for its unique mechanism of action and its effectiveness against various pathogens, particularly gram-negative bacteria. It specifically targets the DXR enzyme in the MEP pathway, which is crucial for isoprenoid

biosynthesis in many gram-negative bacteria (Knak et al., 2022; Kuzuyama et al., 1998). Bacitracin is a polypeptide antibiotic that interferes with phosphorylase activity to prevent the synthesis of peptidoglycans during the second stage of bacterial cell wall synthesis (Vardanyan & Hruby, 2006). Bacitracin has also been demonstrated to effectively prevent invasion and migration of U87-MG glioma cells (Li et al., 2016).

Although targeting mitochondria by OXPHOS inhibitors to overcome chemoresistance seems promising, the efficacy of such drugs can be increased and the overall cytotoxic effect(s) may be reduced (Sandoval-Acuña et al., 2016). Researchers have used triphenylphosphonium (TPP) conjugation techniques to improve the selective delivery of drugs to mitochondria. Since TPP is a lipophilic cation, it accumulates inside mitochondria due to the negative mitochondrial membrane potential (Murphy & Smith, 2007). TPP-conjugated drugs exhibit much better mitochondrial targeting than their unconjugated counterparts; some studies have shown that they can accumulate in the mitochondria 100- to 1000-fold with less systemic impact (Battogtokh et al., 2018).

1.8 Aim of the Study

The main objective of this study was to investigate the effectiveness of selected antibiotics in targeting mitochondrial OXPHOS to overcome drug resistance in TNBC and to identify (possibly) novel mechanisms of such drugs. To achieve this, the first aim was to establish and characterize a cyclophosphamide-resistant TNBC cell line model using MDA-MB-468 cells. Secondly, it was aimed to conduct comprehensive biochemical and molecular analyses to compare the resistant phenotype with its sensitive (parental) counterpart, with a focus on identifying key differences in metabolic pathways, gene expression patterns, and cellular energetics that contributed to chemoresistance. Thirdly, evaluating the therapeutic potential of selected OXPHOS inhibitors, specifically AMX and FSS, was aimed to be investigated on both resistant and sensitive TNBC models, examining their effects on cell viability, metabolism, and the underlying resistance mechanisms. The fourth aim was to explore the efficacy of some novel OXPHOS inhibitors conjugated to TPP, on the parental and resistant TNBC cell models. The fifth aim was to investigate the combinatorial effects of cyclophosphamide and selected OXPHOS inhibitors. Finally, the therapeutic potential of the selected OXPHOS inhibitor was aimed to be studied through in *in vivo* studies with the established resistant cell line.

2. MATERIALS AND METHODS

2.1 Establisment of Cyclophosphamide-Resistant MDA-MB-468 Cell Line

The MDA-MB-468 cells were continuously exposed to cyclophosphamide in order to create cyclophosphamide-resistant cells. First, the IC values were detected by MTT (toxicity) assay, then, following seeding in T25 cell culture flasks, the cells were exposed to IC20 (4,7668 µM) cyclophosphamide for three days. After 3 days, dead cells were eliminated by washing with PBS, and cell media was replaced with fresh media in the absence of cyclophosphamide. The cells were maintained in this media until they began to proliferate and grow again. After that, the media was removed and new media containing IC20 cyclophosphamide was added. At least three repetitions of this cyclophosphamide treatment cycle were conducted. The resistant phenotype of living cells was examined after treatment cycles were completed.

2.2 Cell Maintenance

Parental MDA-MB-468 cells (468-Par) were grown in Dulbecco's modified Eagle's medium (DMEM; Gibco) supplemented with 10% FBS (Fetal Bovine Serum) (Capricorn Scientific) and 1% Penicillin/Streptomycin (Gibco) while IC10 (2,3834 µM) cyclophosphamide was added to the growth media for growing cyclophosphamide-resistant MDA-MB-468 (468-Rcyclo) cells. Both cell lines were incubated at 37 ℃ with %5 CO_2 incubator (Memmert BE500).

2.3 MTT Proliferation Assay

In order to assess cellular metabolic activity, the MTT assay uses the reduction of MTT, a yellow water-soluble tetrazolium dye, to purple-colored formazan crystals, mostly by mitochondrial dehydrogenases (Patravale et al., 2012). The MTT assay was conducted to examine the proliferation and viability of 468-Par and 468-Rcyclo cells alone and treated with several drugs with various concentrations. On the first day, 10^4 cells per well were seeded in 96-well plates and the plates were incubated for 24 hours to allow for cell attachment at 37 ℃ with %5 CO_2 incubator (Memmert BE500). The next day, the cell media were discarded, and the cells were washed with PBS. Then, new media containing increasing concentrations of drugs of interest were added to the wells. After 3 days of incubation with the drugs, the cell media were discarded, and the cells were washed with PBS. Then, the new media supplemented with 0,25 mM MTT solution was added to the cells and incubation at 37 ℃ with %5 CO_2 incubator was done for 4 hours. After that, the cell media were replaced with 150 µL 1:1 ethanol/DMSO solution per well. The plates were mixed briefly in a microplate shaker and using a microplate reader (Tecan Infinite 200Pro), the absorbance values were taken at a wavelength of 570 nm. Finally, GraphPad Prism 10 was used for analysis of the results, and IC50 values were obtained.

2.4 Doubling Time Calculation

To examine the proliferation habits of the parental cells and the 468-Par and 468-Rcyclo cells, their doubling times were calculated. Firstly, 4 x 10^4 cells per well were seeded in 24-well plates (12 groups for 468-Par and 12 groups for 468-Rcyclo cells) and the plates were incubated at 37 ℃ with %5 CO_2 incubator (Memmert BE500). After 21 hours, the cells were collected with 0.25% Trypsin/EDTA solution (Gibco™ Catalog number: 25200056) and counted using a hemacytometer. After a total of 46 hours and 73 hours, the same procedure was carried out. Lastly, the doubling times of the cells were calculated using the formula below:

$$Doubling\ time = \frac{Time\ (in\ hours) \times \ln(2)}{\ln\left(\frac{Number\ of\ cells\ at\ the\ end}{Number\ of\ cells\ at\ the\ beginning}\right)}$$

2.5 Colony Formation Assay

To investigate the ability of the parental cells and the 468-Par and 468-Rcyclo cells to produce a viable colony after treatment with drugs of interest, colony formation assay was conducted. Firstly, 10^3 cells per well were seeded in 6-well plates in triplicates for each group. After incubating the plates at 37 ℃ with %5 CO_2 incubator (Memmert BE500) for 15 days, the cell media were discarded, and the cells were washed with PBS. Cold methanol was used to fix the cells for 15 minutes at -20°C. Following fixation, cells were stained for 15 minutes using a 0.5% Crystal Violet solution. Three PBS washes were performed on the stained cells until no more purple color was visible. Lastly, using ImageJ, the quantity of colonies that formed was measured.

2.6 BCA Assay

Thermo Scientific Pierce BCA Protein Assay Kit was used to measure the amount of protein in the lysed cells. First, the BCA working reagent was prepared by mixing BCA reagents A and B with a ratio of 50:1. Next, 25 µl of samples and standards were added to wells of a 96-well plate using the dilution scheme in Table 2.1. Then, 200 µl of the working reagent was added to each well. After shaking the plate on a microplate shaker and incubating for 30 minutes at 37°C with the plate covered, a microplate reader (Tecan Infinite 200Pro) was used to measure the absorbance values at 562 nm wavelength.

Table 2. 1: BCA standards, dilutions, and concentrations

Standards	Volume of Diluent (µl)	Volume and source of BSA (µl)	Final BSA Concentration (µg/ml)
A	0	300 µl from the stock	2000
B	125	375 µl from the stock	1500
C	325	325 µl from the stock	1000
D	175	175 µl from B	750
E	325	325 µl from C	500
F	325	325 µl from E	250
G	325	325 µl from F	125
H	400	100 µl from G	25
I	400	0	0 (blank)

2.7 Determination of Mitochondrial Complex I Activity

To determine the mitochondrial complex I activity of the 468-Par and 468-Rcyclo cells, Mitochondrial Complex I (NADH-CoQ Reductase) Activity Assay Kit (Elabscience; Catalog No: E-BC-K149-M) was used. The components of the kit are listed in Table 2.2.

Table 2. 2: Mitochondrial Complex I Activity Assay Kit Components

Item	Component
Reagent 1	Extraction solution A
Reagent 2	Extraction solution B
Reagent 3	Protease inhibitor
Reagent 4	Buffer solution
Reagent 5	Substrate A
Reagent 6	Substrate B
Reagent 7	Inhibitor
Reagent 8	Negative reagent

Before starting the experiment, first, reagents were taken to room temperature. 150 µL of double-distilled water was used to dissolve a vial of reagent 5 to obtain the reagent 5 solution. To prepare the reagent 5 working solution, a vial of reagent 5 was dissolved in 15 ml of reagent 4. To prepare the reagent 6 working solution, a vial of reagent 6 was dissolved in 4 ml of anhydrous ethanol, and shaking was done until the solution turned yellow. The reaction working solution was prepared by mixing reagent 6 working solution and reagent 5 working solution in a ratio of 1:59 and kept in ice prior to use. After reagent preparation was completed, the cells were collected and counted, and the desired number of cells (1.5×10^5 cells per group) was resuspended in 3 ml PBS. Then, 100 µl RIPA buffer was added to the cells on ice. After sonicating the cells for 2 minutes, centrifugation was done at 15.000 g for 10 mins at 4℃. The supernatant was discarded, and the precipitate was mixed with 200 µl of reagent 2 and 2 µl of reagent 3. After sonicating the cells for a minute, centrifugation was done at 15.000 g for 10 mins at 4℃. Next, the supernatant was taken for detection and was seeded in a 96-well plate in triplicates for each group. Also, some were taken to determine protein concentration with BCA assay. 3 control wells and sample wells were prepared for each group by adding 20 µl of the supernatant to the wells. Then, 20 µl of reagent 8 was added to the control wells while 20 µl of reagent 7 was added to the sample wells. The wells were mixed completely, and the plate was incubated for 3 minutes at 37 ℃ and after that, 200 µl of reaction

working solution was added to each well. With a microplate reader (Tecan Infinite 200Pro), the absorbance values were measured at a wavelength of 340 nm (A1). 3 minutes later, the absorbance values were measured again at the same wavelength (A2). Finally, mitochondrial complex I activities were calculated using the equation below and GraphPad Prism 10 was used for the analysis of the results:

$$Mitochondrial\ Complex\ I\ Activity\ (U/gprot) = \frac{(A1-A2)_{control}-(A1-A2)_{sample}}{6600\ \times 0.7} \times V_1 \div T \div V_2 \div Cpr \times 10^6$$

6600 : The molar extinction coefficient of NADH, L/(mol.cm)

0.7 : Optical path, cm

V_1 : The volume of the reaction system, 0.24 mL.

V_2 : The volume of the sample, 0.02 mL.

T: The time of reaction, 3 min.

Cpr: The concentration of mitochondria protein in the sample, gprot/L.

10^6 : 1 mol = 10^6 μmol.

2.8 Determination of Mitochondrial Complex II Activity

To determine the mitochondrial complex II activity of the parental and resistant cells, the Mitochondrial Complex II (succinate-coenzyme Q reductase) Activity Assay Kit (Elabscience; Catalog No: E-BC-K150-M) was used. The components of the kit are listed in Table 2.3.

Table 2. 3: Mitochondrial Complex II Activity Assay Kit Components

Item	Component
Reagent 1	Extraction solution A
Reagent 2	Extraction solution B
Reagent 3	Inhibitor
Reagent 4	Buffer solution
Reagent 5	Substrate A
Reagent 6	Substrate B
Reagent 7	Substrate C

Before starting the experiment, first, the reagents were taken to room temperature. To prepare the reaction working solution 150 µL of reagent 4, 20 µL of reagent 6, and 10 µL of reagent 7 were mixed. After that, the cells were collected and counted, and the desired number of cells (1.5 x 10^5 cells per group) was resuspended in 3 ml PBS. Then, 100 µl RIPA buffer was added to the cells on ice. After sonicating the cells for 2 minutes, centrifugation was done at 15.000 g for 10 mins at 4℃. The supernatant was discarded, and the precipitate was mixed with 200 µL of reagent 2 and 10 µL of reagent 3. After sonicating the sample for a minute at 4℃, centrifugation was done at 15.000 g for 10 mins at 4℃. Next, the supernatant was taken for detection. Also, some of the supernatants were taken to determine total protein concentration with BCA assay. Then, 190 µl of reaction working solution was added to each well and the plate was incubated for 3 minutes at 37 ℃. After that, 20 µl of reagent 2 was added to the blank cells and 20 µl of samples from each group were added to the sample wells in triplicates. With a microplate reader (Tecan Infinite 200Pro), the plate was mixed for 3 seconds with a microplate shaker, and the absorbance values were measured at a wavelength of 600 nm (A1). After incubating the plate for 3 minutes at 37 ℃, another measurement was done with the microplate reader at a wavelength of 600 nm (A2). Finally, mitochondrial complex II activities were calculated using the equation below, and GraphPad Prism 10 was used for the analysis of the results:

$$Mitochondrial\ CompleX\ II\ Activity\ (U/gprot) = \frac{[(A1-A2)_{sample} - (A1-A2)_{blank}] \times V_{total}}{V_{sample} \times 21.8^{*} \times T \times Cpr} \times 1000$$

V_{total} : The volume of the reaction system, 0.21 mL.

V_{sample} : The volume of the sample, 0.02 mL.

21.8^{*}: Molar absorption coefficient

T: The time of reaction, 3 min.

Cpr: The concentration of mitochondria protein in sample, gprot/L.

1000: 1 mmol/L = 1000 µmol/L.

To determine the effects of AMX, FSS and TPP-linked bacitracin (TPP-Bac) on the mitochondrial complex II activity of the cells, the cells were treated with their corresponding IC50 values for 3 days prior to the experiment and the same procedure was followed.

2.9 Determination of Mitochondrial Complex IV Activity

To determine the mitochondrial complex IV activity of the 468-Par and 468-Rcyclo cells, Mitochondrial Complex IV (Cytochrome C oxidase) Activity Assay Kit (Elabscience; Catalog No: E-BC-K152-M) was used. The components of the kit are listed in Table 2.4.

Table 2. 4: Mitochondrial Complex IV Activity Assay Kit Components

Item	Component
Reagent 1	Extraction solution A
Reagent 2	Extraction solution B
Reagent 3	Inhibitor
Reagent 4	Substrate
Reagent 5	Stabilizer
Reagent 6	Buffer solution

Before starting the experiment, reagents 1, 2, and 6 were taken to room temperature, whereas reagents 3, 4, and 5 were kept on ice. To prepare an inhibitor working solution, a vial of reagent 3 was dissolved and mixed in 1 ml of anhydrous ethanol. To prepare the substrate working solution, a vial of reagent 4 was dissolved in 4 ml of reagent 6. To prepare a stabilizer working solution, a vial of reagent 5 was dissolved in 200 µl of reagent 6. Lastly, the preparation of the reaction working solution was done by mixing substrate working solution and stabilizer working solution in a ratio of 2000:3. After reagent preparation was completed, the cells were collected, counted and the desired number of cells (1.5×10^5 cells per each group) was resuspended in 3 ml PBS. Then, 100 µl RIPA buffer was added to the cells on ice. After sonicating the cells for 2 minutes, centrifugation was done at 15.000 g for 10 mins at 4℃. The supernatant was discarded, and the precipitate was mixed with 200 µl of reagent 2 and 10 µl of inhibitor working solution. After sonication was done for a minute, centrifugation was done at 11.000 g for 10 mins at 4℃. Then, the supernatant was taken for detection. Also, some were taken to determine protein concentration with BCA assay. After that, 30 µl of reagent 2 was added to the blank cells and 30 µl of samples from each group were added to the sample wells in triplicates. Then, 120 µl of reagent 6 was added to each well and the plate was mixed for 3 seconds with a microplate reader (Tecan Infinite 200Pro). In the last step, 70 µl of reaction working solution to each well, and the absorbance values were measured at a wavelength of 550 nm (A1). After incubating the plate for a minute, another measurement

was done with the microplate reader at a wavelength of 550 nm (A2). Finally, mitochondrial complex IV activities were calculated using the equation below, and GraphPad Prism 10 was used for the analysis of the results:

$$Mitochondrial\ CompleX\ IV\ Activity\ (U/gprot) = \frac{[(A1-A2)_{sample} - (A1-A2)_{blank}] \times V_1}{V_2 \times T \times d \times \in} \div Cpr$$

V_1 : The volume of the reaction system, 0.22 mL.

V_2 : The volume of the sample, 0.03 mL.

∈: Molar absorption coefficient, 0.0191 L/ μmol/cm.

d: Optical path, 0.65 cm

T: The time of reaction, 1 min.

Cpr: The concentration of mitochondria protein in sample, gprot/L.

2.10 Measurement of ATP Content

To determine the ATP content of the 468-Par and 468-Rcyclo cells, the ATP Calorimetric Assay Kit (Elabscience; Catalog No: E-BC-K157-M) was used. The components of the kit are listed in Table 2.5.

Table 2. 5: ATP Calorimetric Assay Kit Components

Item	Component
Reagent 1	Extraction solution A
Reagent 2	Substrate
Reagent 3	Buffer solution
Reagent 4	Enzyme reagent
Reagent 5	Protein precipitator
Reagent 6	Chromogenic agent A
Reagent 7	Chromogenic agent B
Reagent 8	Stop solution
Reagent 9	Standard

Before starting the experiment, reagents were taken to room temperature. To prepare the substrate working solution, a vial of reagent 2 was dissolved in 6 ml of double-distilled water. To prepare the enzyme working solution, a vial of reagent 4 was dissolved in 1.8 ml of double-distilled water. To prepare the control working solution, 100 µl of substrate working solution, 200 µl of reagent 3, and 30 µl of double-distilled water were mixed. To

prepare detection working solution, 100 µl of substrate working solution, 200 µl of reagent 3 and 30 µl of enzyme working solution were mixed. Then, the chromogenic agent was prepared by mixing 75 µl of reagent 6 and 25 µl of reagent 7. Next, 10 mmol/L ATP standard stock solution was prepared by dissolving a vial of reagent 9 in 1 ml of double-distilled water and the stock solution was diluted by taking 30 µl of 10 mmol/L ATP standard stock solution and mixing it with 27 µl of double-distilled water, to obtain 1 mmol/L ATP standard solution. After reagent preparation was completed, the cells were collected and counted and the desired number of cells (1.5×10^5 cells/group) was resuspended in 3 ml PBS. Then, 100 µl RIPA buffer was added to the cells on ice. After sonicating the cells for 2 minutes, centrifugation was done at 15.000 g for 10 mins at 4℃. The supernatant was taken for detection. Also, some were taken to determine protein concentration with BCA assay. For the enzymatic reaction, firstly 4 1.5 ml microcentrifuge tubes were prepared. For the blank tube, 30 µl of 1 mmol/L ATP standard solution was mixed with 330 µl of control working solution. For the standard tube, 30 µl of 1 mmol/L ATP standard solution was mixed with 330 µl of detection working solution. For the control tube, 30 µl of sample supernatant was mixed with 330 µl of control working solution. For the blank tube, 30 µl of sample supernatant was mixed with 330 µl of detection working solution. All these tubes were mixed completely and incubated for 30 minutes at 37 ℃. To each tube, 50 µl of reagent 5 was added and centrifugation was done at 10.000 g for 5 mins. Then, 60 µl of supernatant was added to the wells for each group in triplicates. After that, 100 µl of the chromogenic agent was added to each well and the plate was mixed for 5 seconds. Incubation was done for 2 minutes at room temperature, 100 µl of reagent 8 was added to each well and the plate was mixed for 5 seconds with the microplate reader. Incubation was done for 5 minutes at room temperature and the absorbance values were measured at a wavelength of 636 nm with the microplate reader. Finally, the ATP content of the samples was calculated using the equation below, and GraphPad Prism 10 was used for the analysis of the results:

$$ATP\ content\ (mM) = \frac{OD_{sample} - OD_{control}}{OD_{standard} - OD_{blank}} \times c$$

c: Concentration of standard (1 mmol/L)

To determine the effects of AMX, FSS, and TPP-Bac on the ATP content of the cells, the cells were treated with their corresponding IC50 values for 3 days prior to the experiment and the same procedure was followed.

2.11 MitoTracker Mitochondrial Staining Assay

To determine the mitochondrial mass of the 468-Par and 468-Rcyclo cells, MitoTracker Green FM (Mitogreen) (Invitrogen™ M7514) dye was used. Firstly, 2×10^4 cells from each group were seeded on a 96-well plate in triplicates and incubation was done for 1-2 hours at 37 ℃ to allow for cell attachment (Memmert BE500). Then, media containing mitogreen was prepared by mixing %1 mitogreen with normal growth media in a ratio of 3:320. The cell media was replaced with this mitogreen-containing media and incubation was done at 37 ℃ with %5 CO_2 incubator was done 25 minutes. Then, cell media was removed and washed with media non-supplemented with Penicillin/Streptomycin. After incubating the plate for 5 minutes at 37 ℃ with %5 CO_2 incubator, the washing step and incubation was repeated. Lastly, the cell media was removed, 50 µl of PBS was added to each well and the fluorescent measurement was done using a spectrophotometer (Molecular Devices, SpectraMax Gemini™ XPS/EM) at an excitation wavelength of 490 nm and emission wavelength of 510 nm. GraphPad Prism 10 was used for analysis of the results. To determine the effects of AMX, FSS and TPP-Bac on the mitochondrial mass of the cells, the cells were treated with their corresponding IC50 values for 3 days prior to the experiment and the same procedure was followed.

2.12 JC-1 Staining

To assess changes in the mitochondrial membrane potential of the 468-Par and 468-Rcyclo cells, which is an indicator of mitochondrial health, JC-1 dye (Invitrogen™T3168) was used. In healthy cells with high mitochondrial membrane potential, JC-1 forms aggregates and emits red fluorescence, whereas, in cells with low membrane potential, JC-1 remains in its monomeric form and emits green fluorescence. Firstly, 1 µl from a stock solution of 1mg/ml JC-1 dye in DMSO was taken and mixed with 100 µl of DMEM phenol red (Gibco) to achieve a final concentration of 5 µg/ml. Then, this solution was sonicated for 3-5 minutes by shaking periodically. 2×10^5 cells from each group were seeded on a 96-well plate in triplicates and 50 µl of the prepared JC-1 solution was added to each well. After incubating the plate for 10-30 minutes at 37 ℃ with %5 CO_2 incubator (Memmert BE500), the media was replaced with 50 µl of fresh DMEM colorless (no phenol red; Gibco) for 2 times by 1 minute each. Lastly, the

measurement was done using a spectrophotometer (Molecular Devices, SpectraMax Gemini™ XPS/EM) at an excitation wavelength of 514 nm and emission wavelength of 529 nm for the detection of JC-1 monomers and at an excitation wavelength of 514 nm and emission wavelength of 590 nm for detection of JC-1 aggregates. GraphPad Prism 10 was used for analysis of the results.

To determine the effects of AMX and FSS on the mitochondrial membrane potential of the cells, the cells were treated with their corresponding IC50 values for 3 days prior to the experiment and the same procedure was followed.

2.13 Gelatin Zymography

For the determination of the matrix metalloproteinase (MMP) activity and metastatic ability of the 468-Par and 468-Rcyclo cells, gelatin zymography was conducted. Firstly, 2×10^5 cells were seeded on 6-well plates in triplicates for each group. After cells had reached 70-80% confluency, cell media was replaced with FBS-free media. In this step, IC50 concentrations of AMX, FSS, and TPP-Bac drugs were added to the cells. The plates were incubated overnight at 37 ℃ with %5 CO_2 incubator. The next day, polyacrylamide separating and stacking gels were prepared with the ingredients listed in Table 2.6. After preparation, the gels were poured between the glasses in the cast system, a comb was placed and the gels were polymerized.

Table 2. 6: The ingredients of gelatin zymography separating and stacking gels

Ingredients	Separating gel	Stacking gel
dH_2O	2 mL	3.075 mL
Gelatin (4 mg/ml)	2 mL	-
Acrylamide / Bisacrylamide (1:29)	2 mL	670 µL
1.5M Tris-HCl pH: 8.8	2 mL	-
0.5M Tris-HCl pH: 6.8	-	1.25 mL
10% SDS	80 µL	50 µL
10%APS	80 µL	50 µL
TEMED	10 µL	10 µL

Glass plates were then inserted into the electrode assembly and placed into the electrophoresis tank system, and 1X running buffer diluted from 10X running buffer (Table 2.7) was added to the tank.

Table 2. 7: The components of the 10X running buffer

Ingredients	Amount
Tris Base	30.285 g
Glycine	144.4 g
SDS	10 g
dH_2O	1 L

After that, incubated cell media was collected from every group and centrifuged to concentrate. 40 µl of these concentrated media was then mixed with 10 µl of 5X non-reducing sample buffer (Table 2.8). 22 µl from each of these mixtures and 5 µl of protein ladder (3-color Prestained Protein Marker 10-190 kDa Cat#HY-K1011 Medchemexpress) were loaded into the gel and running the gel was done at 40V for 15 minutes and after that, the voltage was increased to 140V for 50 minutes (BIORAD Mini Protean Tetra System).

Table 2. 8: The ingredients of 5X non-reducing sample buffer solution

Final Concentration	For 50 ml
125 mM Tris-HCl, pH 6.8	12.5 ml (from 0.5M)
20% Glycerol	20 ml (from 50%)
4% SDS	20 ml (from 10%)
0.01% Bromophenol Blue	0.005 g

After running was completed, the gels were placed on a shaker (Stuart gyro-rocker SSL3) in the washing buffer (Table 2.9) to eliminate excess SDS by agitation. This washing step was repeated 4 times in 20-minute intervals.

Table 2. 9: The ingredients of the washing buffer solution

Final Concentration	For 250 ml
2.5% Triton X-100	6.25 ml (from 100%)
50 mM Tris-HCl, pH 7.5	12.5 ml (from 1M)
5 mM $CaCl_2$	625 µl (from 2M)
1 µM $ZnCl_2$	2.5 µl (from 0.1M)

Next, the incubation of the gels was done for 10 minutes at room temperature in the Triton X-100-containing incubation buffer (Table 2.10). After replacing it with a fresh incubation buffer, incubation was done overnight at 37 ℃ with %5 CO_2 incubator (Memmert BE500).

Table 2. 10: The ingredients of the incubation buffer solution

Final Concentration	For 250 ml
1% Triton X-100	2.5 ml (from 100%)
50 mM Tris-HCl, pH 7.5	12.5 ml (from 1M)
5 mM $CaCl_2$	625 µl (from 2M)
1 µM $ZnCl_2$	2.5 µl (from 0.1M)

After overnight incubation was completed, gel staining was done by placing the gels on the shaker in the staining solution (Table 2.11). The staining was completed in 1-2 hours with slow agitation and the gels were washed with water twice.

Table 2. 11: The ingredients of the staining solution.

Ingredients	For 100 ml
Methanol	40 ml
Acetic Acid	10 ml
H_2O	50 ml
Coomassie Blue	0.5 g

Next, the gels were placed on the shaker in the destaining solution (Table 2.12) and the solution was replaced with a fresh destaining solution every once in a while when the solution turned blue. This step was repeated until clear bands were visible on the gels. Lastly, ImageJ was used to determine band intensities, and GraphPad Prism 10 was used to analyze the results.

Table 2. 12: The ingredients of the destaining solution.

Ingredients	For 1 L
Methanol	400 ml
Acetic Acid	100 ml
H_2O	500 ml

2.14 RNA Isolation

To isolate RNA from the 468-Par and 468-Rcyclo cells, QuickEX Total RNA Extraction Kit (Nucleogene, Turkey) was used. The components of the kit are lysis buffer, wash buffer I, wash buffer II, DNAse I, DNAse I buffer, elution buffer, spin columns, and collection tubes. The cells were treated with corresponding IC50 values of AMX and FSS for 3 days prior to the experiment. For the experiment, treated and non-treated cells were collected and counted. Also, MDA-MB-468 CSCs were collected and counted. 1×10^6 cells were used for RNA isolation and centrifugation of the samples at 300g for 5 minutes was done. Then, cell lysis was done with 600 µl lysis buffer and the cells were incubated for 10 minutes at room temperature. Centrifugation was done in a microcentrifuge for 2 minutes at 14.000g. The supernatant was carefully taken and 400 µl of pure ethanol (Merck) was added to 400 µl of supernatant. After vortexing the mixture for 1 minute, the sample was transferred into a spin column in a collection tube. Centrifugation was done at 11.000g for 30 seconds and the collection tube was then discharged. 5 µl of DNase I (6 U/I) and 45 µl of DNase I buffer were mixed gently and transferred to the column matrix for each sample. After incubating this mixture for 15 minutes at room temperature, 400 µl of wash buffer I was added to the columns. Centrifugation was done at 11.000g for 30 seconds and the collection tube was then discharged. This step was done twice. Then, 700 µl of wash buffer II was added to the columns. Centrifugation was done at 11.000g for 1 minute and the spin column was placed in a new tube. The elution of RNA was done by adding 100 µl of elution buffer to the column center and centrifugation was done at 11.000g for 2 minutes. Lastly, RNA concentration and purity were determined with a NanoDrop UV/Vis Spectrophotometer (Thermo Scientific NanoDrop 2000).

2.15 cDNA Synthesis

From the isolated RNA samples, cDNA synthesis was done with Nucleogene cDNA Synthesis Kit (5X) (Nucleogene, Turkey). In this kit, a reaction buffer consisting of optimized concentrations of recombinant RNAse inhibitor protein, dNTPs, stabilizers, $MgCl_2$ and qScript reverse transcriptase, was provided. For cDNA synthesis, 100 ng of isolated RNA from each sample was calculated and used. The reaction assembly for the cDNA synthesis is shown in Table 2.13.

Table 2. 13: The reaction assembly for the cDNA synthesis

Component	Volume / Amount
Reaction Buffer (5X)	4 µl
Water (Rnase/Dnase-free)	Variable
RNA	100 ng
Total volume:	20 µl

These components were kept on ice, mixed, and then, centrifuged shortly. After that, the incubation conditions shown in Table 2.14 were done with a thermocycler (Bio-Rad; C1000 Touch Thermal Cycler).

Table 2. 14: The incubation conditions for cDNA synthesis

Step	Temperature	Time
1	25 ℃	5 minutes
2	50 ℃	30 minutes
3	85 ℃	5 minutes
4	4 ℃	Storage

2.16 Real Time Quantitative PCR (RT-qPCR)

3 µl from the synthesized cDNA templates was used for RT-qPCR using Nucleogene qPCR SYBR Green Master Mix (2X) (Nucleogene, Turkey). 2X reaction buffer consists of hot-start DNA polymerase, inhibitory activators, dNTPs, stabilizers, $MgCl_2$, and SYBR green dye. For PCR amplification, the reaction assembly in Table 2.14 was followed.

Table 2. 15: The reaction assembly for PCR amplification

Component	Volume
Nucleogene qPCR SYBR Green Master Mix (2X)	10 µl
Forward Primer	0.3 µl
Reverse Primer	0.3 µl
Nuclease-free Water	7.4 µl
cDNA template	2 µl
Total volume:	**20 µl**

The forward and reverse primers (Nuclogene, Turkey) used for the detection of Sox-2 and Nanog genes in the samples are given in Table 2.15.

Table 2. 16: The forward and reverse primers used in RT-qPCR

Nanog Forward Primer	TCTGGACACTGGCTGAATCCT
Nanog Reverse Primer	CGCTGATTAGGCTCCAACCAT
Sox-2 Forward Primer	GCTCGCAGACCTACATGAAC
Sox-2 Reverse Primer	GGGAGGAAGAGGTAACCACA

The components were mixed and then, centrifuged shortly. Then, 20 µl of the PCR reaction mixture was loaded into a 96-well reaction plate for each sample and gene. The plate was sealed to cover, and the plate was centrifuged shortly. The plate was placed into the device (Roche; LightCycler 480 II) for conducting cycling reactions (Table 2.16). Lastly, GraphPad Prism 10 was used for analysis of the results.

Table 2. 17: RT-qPCR reaction steps

Steps	Temperature	Time
Initial Denaturation	95°C	15 min
Denaturation	95°C	15 sec (45 cycles)
Annealing	60 °C	30 sec (45 cycles)
Extension / Elongation	72 °C	10 sec (40 cycles)

2.17 Determination of Oxygen Consumption Rate

A Clark-type oximeter (Hansatech Oxygraph+, U.K.) was used to measure the oxygen consumption rate (OCR) of the 468-Par and 468-Rcyclo cells. To maintain a constant temperature inside the chambers during measurements, the chambers where the cell samples would be added were connected to a water bath set at 37℃. Firstly, the device was prepared for sample addition. To do that, on the top and sides of the electrode, four drops of KCl solution were applied and a membrane covering the electrode disc and a thin piece of cigarette paper were placed on top of the electrode. After securing the cigarette paper and membrane to the electrode with a rubber disk, the electrode was linked to a sensor device and when the oxygen signal was stabilized, the electrode was connected to the chamber. Before adding the sample, the magnetic stirrer speed of the oximeter was

adjusted by adding deionized water to the chamber and after that, the water was removed and 600 µl PBS, that was heated to 37℃ before, was added to be used as the blank measurement. To measure the oxygen consumption rate of two groups of cells, these procedures were carried out simultaneously for two electrodes and two devices. After blank measurement was done, which was understood from the constant oxygen signal, PBS was removed and cell samples were added to the chambers. 3×10^6 of parental and cyclophosphamide-resistant MDA-MB-468 cell pellets were suspended in 600 µl PBS and added to separate chambers. A plugger with a thin, sealable hole was used to close the chambers and for 35 minutes, the oxygen content of the samples was monitored. Next, 20 µl of ADP (Sigma Aldrich A2754), which acts as a substrate for mitochondrial respiration, was added to the samples from the hole in the plugger, and for 40 minutes, the oxygen content of cell samples was monitored. Then, 20 µl of FCCP (Medchemexpress HY-100410) was added to the samples and for 40 minutes, the oxygen content of cell samples was monitored. In order to stop respiration, 20 µl of rotenone was finally added to cell samples. For the purpose of analyzing protein expression by Western blotting, the cells were taken out of the chambers and kept in 70 uL of RIPA buffer at -80℃. Hansatech's Oxytrace+ software was used to calculate the oxygen consumption rate. Plotting of the OCR/time graphs was done using GraphPad Prism 10.

To determine the effects of AMX and FSS on the OCR of the cells, the cells were treated with their corresponding IC50 values for 3 days prior to measurement, and the same measurement steps were followed.

2.18 Western Blot

Triple-negative breast tumor (TNBT) patient samples and minimal data annotation included in this study were provided by the Tumor Bank of Vall d'Hebron University Hospital Biobank (PT13/0010/), integrated in the Xarxa de Bancs de Tumors de Catalunya, and were processed following standard operating procedures with the appropriate approval of the Ethical and Scientific Committees. 8 of 12 samples were processed as they showed uniform distribution of cell mass with minimal fat content. Samples were stored on dry ice, homogenized with a pestle, and lysed with RIPA buffer (0.5 M Tris-HCl, pH 7.4, 1.5 M NaCl, 2.5% deoxycholic acid, 10% NP-40, 10 m M EDTA, 2% SDS). After sonication on ice (30 bursts for 20 seconds each) and

centrifugation at 4C at 15000 RPM, supernatants were collected, and some were taken to determine protein concentration with BCA assay. After determination, the amount of sample corresponding to 20 µg total protein concentration was calculated for each sample. Next, the calculated amounts of samples were taken and mixed with 5X Laemmli buffer (Table 2.17) with a ratio of 1:4. The samples were boiled at 95℃ for 3 minutes.

Table 2. 18: The ingredients of the 5X Laemmli Buffer

Laemmli Buffer (5X)	Amount
SDS	0.5 g (5%)
Glycerol	5 ml (50%)
β-mercaptoethanol	0.5 ml
Tris-HCl (0.5M pH:6.8)	5 ml
Bromophenol Blue	1 mg

Then, the gel preparation was carried out. The running gel and the stacking gel (Table 2.18) were prepared and the gels were left to polymerize after being poured between the glasses in the cast system. After the electrophoresis tank system was assembled, it was filled with 1X running buffer that had been diluted from 10X running buffer (Table 2.7). Then, the samples and the 5 µl of protein ladder (3-color Prestained Protein Marker 10-190 kDa Cat#HY-K1011 Medchemexpress) were loaded into the gel, and running the gel was done at 50V for 5 minutes and after that, the voltage was increased to 140V for 1 hour (BIORAD Mini Protean Tetra System).

Table 2. 19: The ingredients of the running gel and stacking gel for the western blot

Ingredients	Running gel	Stacking gel
Distilled water	4.1 ml	2.7 ml
Acrylamide/Bisacrylamide (1:29)	3.3 ml	0.8 ml
Tris-HCl (1.5 M) pH:8.8	2.5 ml	-
Tris-HCl (0.5 M) pH:6.8	-	0.5 ml
SDS (20%)	50 µL	20 µL
APS (10%)	100 µL	40 µL
TEMED	10 µL	4 µL

After the running was completed, the gels were incubated in a transfer buffer for 10-15 minutes. For protein transfer, 6 filter papers and 1 PVDF membrane were cut, and the membrane was soaked in methanol for 15 seconds. Then, sponges, filter papers, and a membrane were placed in a transfer buffer to keep them wet. The transfer sandwich cassette was assembled in layers in the following order: Sponge, 3 filter papers, the gel, membrane, 3 filter papers, and another sponge. The cassette was placed in the electrophoresis tank and also, an ice block was put in. The protein transfer was conducted for 1-1.5 hours at 90-110V in 1X transfer buffer (Table 2.19). After that, the membranes were blocked for 40 minutes in TPBS/5% milk to prevent non-specific binding of antibodies to the membrane on a shaker (Stuart gyro-rocker SSL3) and kept wet-frozen at -20℃.

Table 2. 20: The transfer buffer ingredients for the protein transfer procedure in western blot

Ingredients	Amount	Final Concentration
Tris Base	15 g	1.5% (v/v)
Glycine	2.9 g	0.29% (v/v)
SDS	0.37 g	0.037% (v/v)
Methanol	200 ml	20% (v/v)
dH2O	800 ml	

For the immunoblotting procedure, the membranes were taken, and they were incubated with primary antibody for 1 hour at room temperature on a shaker (Stuart gyro-rocker SSL3). Then, the membranes were washed for 3 times up to 10 minutes with PBS-T (0.5 mL Tween-20 in 1 L1X PBS). The membranes were taken, and they were incubated on a shaker with a secondary antibody for an hour at room temperature. After washing the membranes for 3 times up to 10 minutes with PBS-T, the protein bands on the membrane were detected with Gel Doc EZ Imager (Bio-Rad).

2.20 Combinatorial Treatment

The effects of combining cyclophosphamide with antibiotics AMX, FSS, and TPP-Bac on the 468-Par and 468-Rcyclo cells' survivability were investigated with the MTT assay. The experimental setup is given in Figure 2.1. This setup was done for each type of antibiotic. GraphPad Prism 10 was used for analysis of the results.

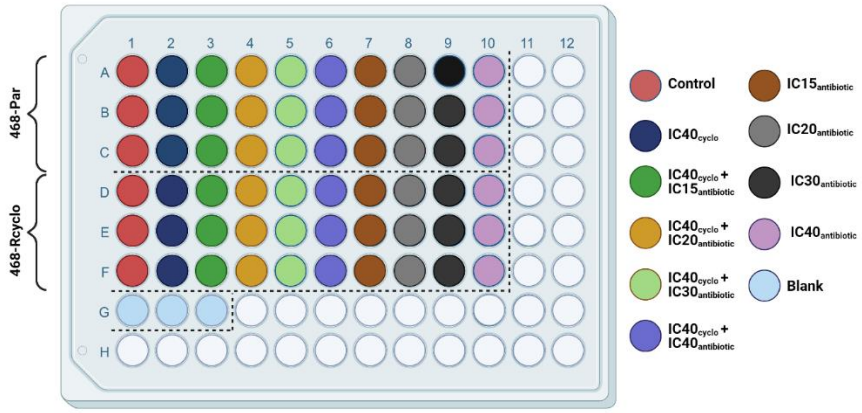

Figure 2. 1: The experimental setup for the combinatorial treatment.
The combinatorial treatment of the 468-Par and 468-Rcyclo cells with cyclophosphamide and antibiotics AMX, FSS and TPP-Bac. This figure is created with Biorender.com.

2.21 *In vivo* Animal Studies

8-week female NMRI-nu mice were purchased from Janvier Labs (France) and housed in a pathogen-free environment. Power analysis using data from the pilot experiment showed that 4 mice per group would provide 80% power to detect differences in the % of resistant cells in the drug-treated groups at $p < 0.05$. Animals were s.c. inoculated in the flank with $1x10^6$ cells mixed 1:1 with matrigel. Mice were housed in groups of 6 in cages with drinks *ad libitum* and regular feeding and randomly assigned to treatments. Weight and tumor growth were measured with a caliper and using the formula [length x width x height(mm)]/2 were followed weekly. When tumors reached a size > 100 mm^3, they were randomized into different groups and treated with vehicle or Amx at a concentration of 100 mg/kg in drinking water twice a week. Mice were then separated into four distinct cages, 6 mice per each: the control groups of mice with 468-Par and with 468-Rcyclo and the experimental groups of mice with 468-Par and with 468-Rcyclo that were treated bi-weekly with AMX dissolved in drinking water.

Also, 8 mice were injected with CSC and after the injection, the mice were housed with free access to water and food. Ten days later, based on their tumor volumes, the mice were randomized into two groups containing 4 mice each: the control group of 468-CSC mice and the experimental group of 468-CSC mice treated with AMX in drinking water once a week. At the end of treatment, mice were sacrificed, and tumors were harvested and measured for size. GraphPad Prism 10 was used for the analysis of the results.

2.22 CSC Obtainment

1.5×10^3 cells pretreated with DMSO or IACS alone or in combination with cisplatin (cisplatin, 6 μM; IACS-010.759, 1 μM) for 3 h were seeded in 24-well low attachment plates (Corning, 3473) in stem cell medium [DMEM-F12 (Corning, #10-017-CV) with 100 U penicillin-streptomycin, 0. 4% BSA, 10 ng/mL bFGF (Invitrogen, #13256-029), 20 ng/mL EGF (Biolegend, 585,506), 5 μg insulin (Sigma, 19278)]. The plates were incubated for 14 days at 37 °C, 5% CO2. Fresh stem cell medium was added every 3 days and spheroids were visualized after 14 days. Whenever necessary, drug treatment with IC 30 was performed and compared to untreated (control) samples. The microscopic images of the 3d generation spheroids were made with a Zeis microscope (x20) and the exact numbers in each well were calculated manually followed by plotting to a graph was plotted.

3. RESULTS

3.1 Establishment of the Chemoresistant TNBC Cell Line Model

In this study, it was first aimed to establish and characterize a chemoresistant TNBC cell line using cyclophosphamide on MDA-MB-468 cells to get a fundamental model for studying drug resistance mechanisms. For this aim, MDA-MB-468 cells were continuously exposed to increasing concentrations of cyclophosphamide over several months, following a previously established protocol (Cinatl et al., 2024). The resistant phenotype was confirmed through multiple approaches. Initially, doubling times for both 468-Par and 468-Rcyclo were calculated with a doubling time assay. It was revealed that 468-Rcyclo cells exhibited a faster proliferation rate compared to parental cells. For the resistant cells, the doubling time was determined to be 16.03 ± 1.2 hours, whereas parental cells had a longer doubling time of 46 ± 0.57 hours (Figure 3.1.1A). This observation suggests that the resistant phenotype may have adapted to proliferate more rapidly, potentially utilizing alternative metabolic pathways to support this increased growth rate. This aligns well with previous studies showing metabolic adaptations in chemoresistant cancer cells that can lead to enhanced proliferation capacity (Birsoy et al., 2015; Vasan et al., 2020).

Morphological examination revealed distinct characteristics in resistant cells compared to their parental counterparts. 468-Rcyclo cells exhibited a more elongated, mesenchymal-like morphology with increased cell spreading, whereas parental cells maintained their typical epithelial-like appearance (Figure 3.1.1B). These morphological changes suggest potential epithelial-to-mesenchymal transition (EMT) features in resistant cells. To confirm the establishment of the resistant phenotype, an MTT cell viability assay was conducted and revealed a significant increase in the IC50 value for

cyclophosphamide in resistant cells (11.917µM) compared to parental cells (3.989µM), indicating approximately 3-fold resistance (Figure 3.1.1C). This resistance remained stable even after multiple passages in a drug-free medium, suggesting the establishment of a stable resistant phenotype. This level of resistance is consistent with previous studies establishing chemoresistant breast cancer cell lines (Tsou et al., 2015; Wu et al., 2019).

A

Cell Line	Doubling Time (hours)
MDA-MB-468 parental cells	16.03 ± 1.2
MDA-MB-468 cyclophosphamide-resistant cells	46 ± 0.57

B

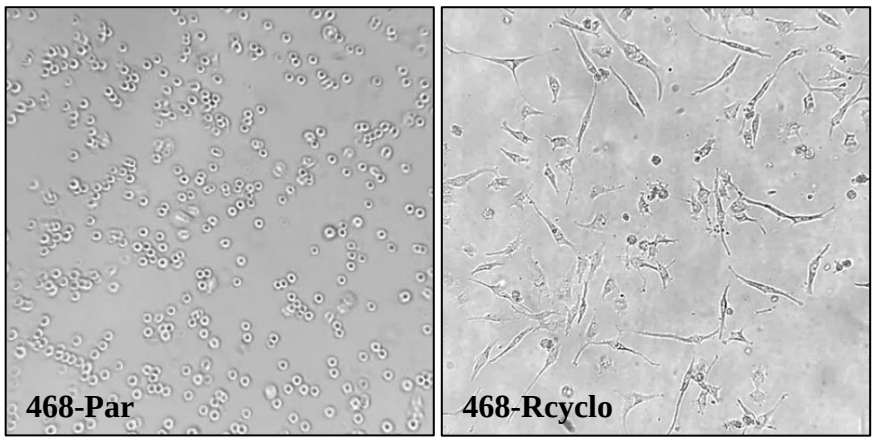

C

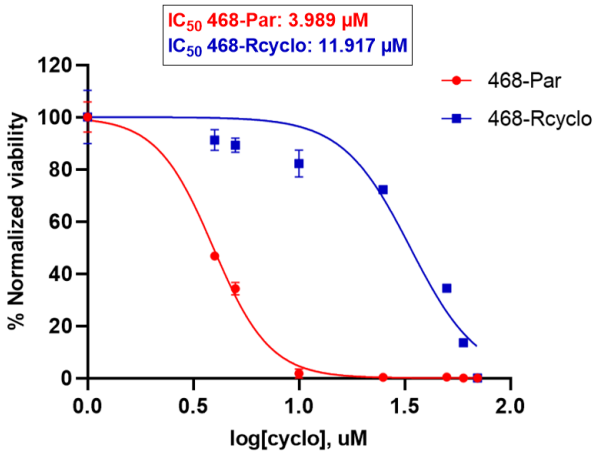

Figure 3. 1.1: The establishment of a chemoresistant TNBC cell line model.

(A) The doubling times for MDA-MB-468 parental (468-Par) and cyclophosphamide-resistant cells (468-Rcyclo) were calculated by seeding, incubating, and counting the cells simultaneously after 21, 46, and 73 hours. The doubling times were calculated with the following formula: Doubling time = (t x ln2)/[ln(N_0/N_t)] where N_t is the cell count at time t, and N_0 is the initial cell count. ***(B)*** The cell morphological differences were observed under a phase-contrast microscope. ***(C)*** The viability difference between 468-Par and 468-Rcyclo was identified by MTT assay and the corresponding IC50 values for cyclophosphamide were calculated. Cells (10^4 per well) were seeded and incubated for 24 hours at 37°C for cell attachment. The media was then discarded, and new media containing increasing concentrations of cyclophosphamide were added, followed by a 3-day incubation. Afterward, the media were replaced with 0.25 mM MTT solution for 4 hours. The media were then changed to a 1:1 ethanol/DMSO solution, and absorbance was measured at 570 nm using a microplate reader. Statistical analyses were done, and graphs were prepared by using GraphPad Prism 10. Each value represents the mean ± SD of three replicates analyzed by Student t-test ($p < 0.01$).

3.2 Enhanced Mitochondrial Function Elevates ATP Levels in Drug-Resistant Cancer Cells

Acquired drug resistance is often associated with significant alterations in cellular metabolism, particularly in mitochondrial function and energy production pathways (Vyas et al., 2016). To characterize the metabolic profile of resistant cells, comprehensive analyses of mitochondrial function and energy metabolism were performed in both parental and resistant cell lines.

Examination of mitochondrial respiratory chain complexes revealed significant differences between resistant and parental cells. Calorimetric analysis showed that the activity of complex II was increased 2.3-folds in 468-Rcyclo cells compared to parental cells, while the activities of complexes I and IV were not significantly different (Figure 3.2.1A). These results are consistent with previous studies showing increased mitochondrial respiratory chain activity in chemoresistant cancer cells (Vyas et al., 2016). Cellular ATP levels, measured using a calorimetric assay, were significantly higher in resistant cells (0.6767 ± 0.018 mM) compared to parental cells (0.3724 ± 0.026 mM) (Figure 3.2.1B). This increased ATP production correlates with the enhanced mitochondrial complex II activity and suggests a shift toward increased oxidative phosphorylation, a phenomenon previously observed in another TNBC line (Uslu et al., 2024).

To further characterize mitochondrial alterations, mitochondrial mass was assessed using MitoTracker Green FM, a fluorescent dye that specifically labels mitochondria regardless of membrane potential (Lang et al., 2016). Spectrophotometric analysis revealed that 468-Rcyclo cells exhibited significantly higher mitochondrial mass, with a 2.4-fold increase in MitoTracker Green fluorescence intensity compared to parental cells (Figure 3.2.1C). This increase in mitochondrial mass suggests enhanced mitochondrial biogenesis, which often correlates with increased metabolic capacity and drug resistance (Bokil & Sancho, 2019). The results are also consistent with studies showing that mitochondria improve cancer cells' ability to adapt to stressors by reprogramming their abundance (Henkenius et al., 2017; H. Wang et al., 2020).

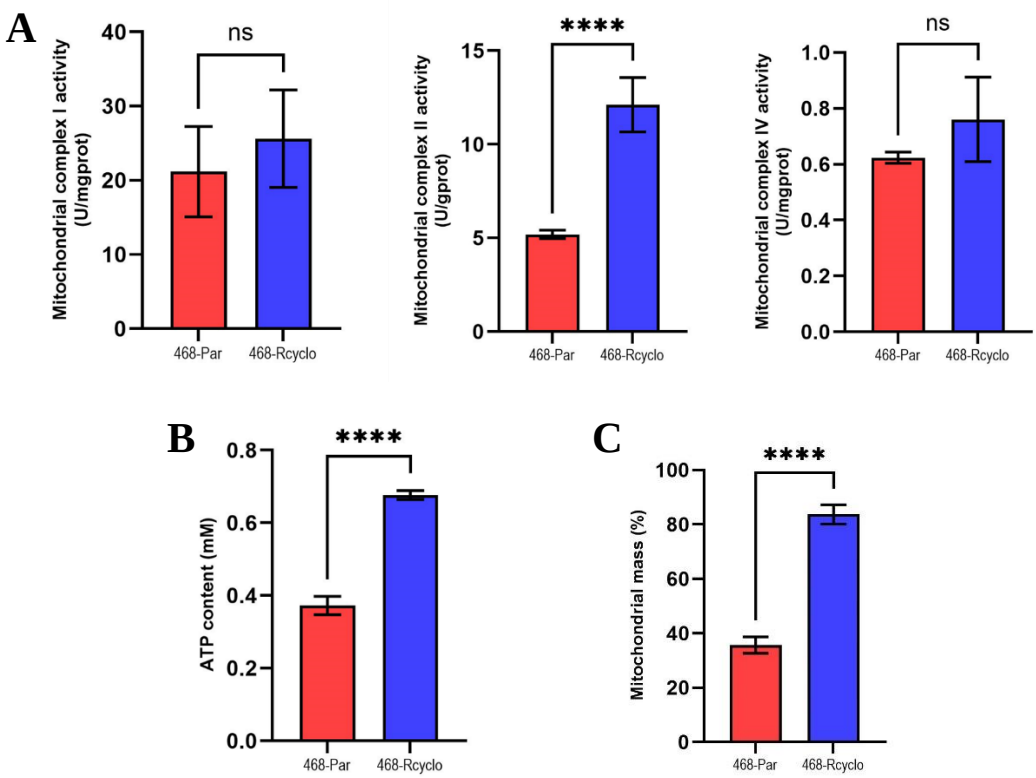

Figure 3. 2.1: Enhanced mitochondrial function elevates ATP levels in 468-Rcyclo.
(A) The mitochondrial complexes I, II, and IV activities of 468-Par and 468-Rcyclo cells were done by calorimetric assays, according to the manufacturer's protocols (Elabscience; E-BC-K149-M, E-BC-K150-M, E-BC-K152-M). ***(B)*** The ATP content of 468-Par and 468-Rcyclo cells was calculated by ATP calorimetric assay, according to the manufacturer's protocol (Elabscience; E-BC-K157-M). ***(C)*** The mitochondrial mass of the 468-Par and 468-Rcyclo cells was determined with MitoTracker Green FM (Invitrogen™ M7514) dye. After incubating the cells in 1% dye-containing media for 25 minutes, fluorescent measurement was done with a spectrophotometer at an excitation wavelength of 490 nm and emission wavelength of 510 nm. Statistical analyses were done, and graphs were prepared by using GraphPad Prism 10. Each value represents the mean ± SD of three replicates analyzed by Student t-test. *p<0.05, **p<0.01, ***p<0.001, ****p<0.0001, ns: non-significant.

When evaluating mitochondrial function in relation to the ability of the mitochondria to generate ATP through OXPHOS, the mitochondrial membrane potential is frequently measured (Shao et al., 2018). Mitochondrial membrane potential, assessed using JC-1 staining, showed a 1.4-fold increase in the red/green fluorescence ratio in resistant cells (Figure 3.2.2A), indicating higher mitochondrial membrane depolarization. This observation is consistent with previous reports linking decreased mitochondrial membrane potential to chemoresistance (Caino et al., 2015). Furthermore, the observed decrease in membrane potential correlates strongly with our findings of increased ATP production. In normal cells, a drop in mitochondrial membrane potential triggers mitophagy. These results suggest that resistant cells continue functioning despite lower membrane potential, effectively evading mitophagy signals while maintaining OXPHOS activity (Bokil & Sancho, 2019; Sivandzade et al., 2019). This metabolic adaptation appears to confer improved survival mechanisms.

Oxygen consumption rate (OCR) measurements using a Clark-type oximeter (Hansatech Oxygraph+) demonstrated significantly higher basal respiration in resistant cells compared to parental cells (Figure 3.2.2B). The mitochondrial respiratory capacity, observed after ADP addition, was also notably higher in resistant cells, suggesting enhanced metabolic flexibility. Drug-resistant cancer cells are known to have reprogrammed their metabolism, resulting in a shift in energy metabolism toward OXPHOS (M. Lee et al., 2019). Therefore, this result confirmed the metabolic reprogramming of 468-Rcyclo cells toward OXPHOS.

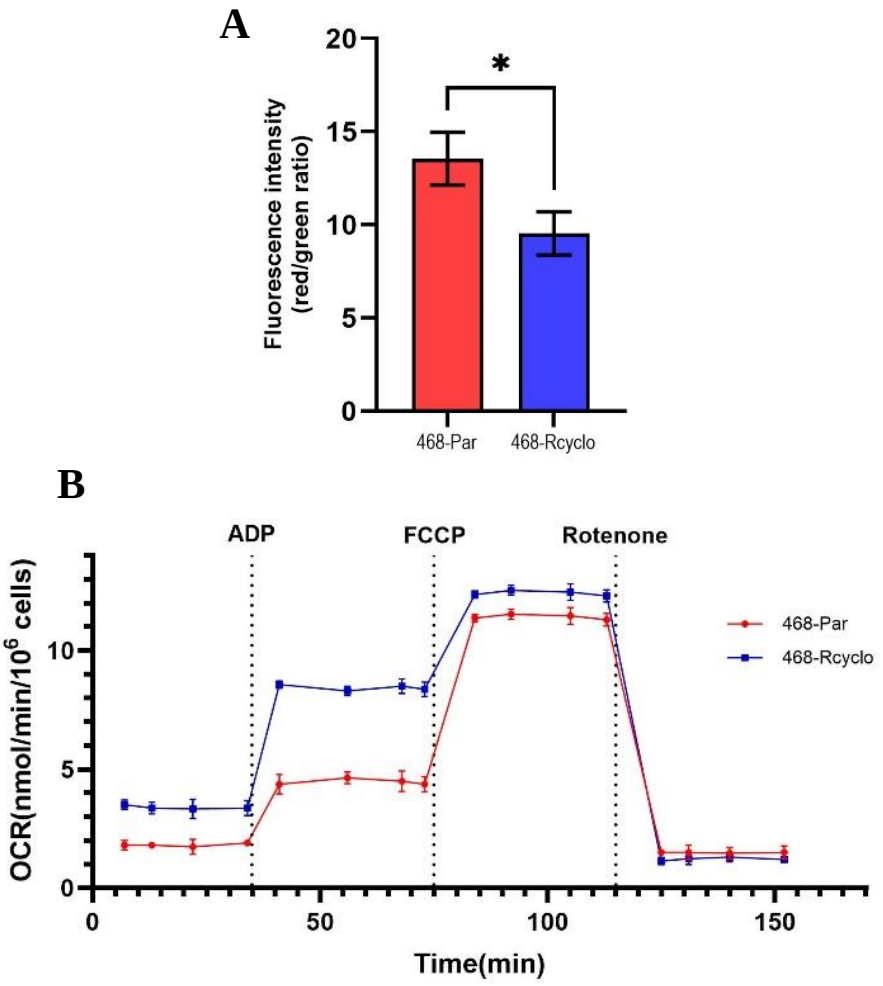

Figure 3.2.2: Drug-resistant cancer cells exhibit increased oxygen consumption and mitochondrial membrane depolarization.

(A) Changes in mitochondrial membrane potential of the 468-Par and 468-Rcyclo cells were determined with JC-1 dye (Invitrogen™T3168). After incubating the cells in 5 µg/ml of JC-1 dye solution for 10 minutes, fluorescent measurement was done with a spectrophotometer twice, at an excitation wavelength of 514 nm and emission wavelength of 529 nm for detection of JC-1 monomers and at an excitation wavelength of 514 nm and emission wavelength of 590 nm for detection of JC-1 aggregates. ***(B)*** The oxygen levels of 3×10^6 of 468-Par and 468-Rcyclo cell pellets suspended in 600 µl PBS were monitored without and with the addition of 20 µl ADP, 20 µl FCCP, and 20 µl rotenone with a clark-type oximeter (Hansatech Oxygraph+). Statistical analyses were done, and graphs were prepared by using GraphPad Prism 10. Each value represents the mean ± SD of three replicates analyzed by Student t-test. *p<0.05, **p<0.01, ***p<0.001, ****p<0.0001, ns: non-significant.

3.3 Drug-Resistant Cancer Cells Show Higher Sensitivity to Antibiotics

After identifying the metabolic changes in resistant and parental cells, the therapeutic potential of two antibiotics, AMX and FSS, targeting mitochondrial function in both parental and resistant cell lines was investigated. AMX and FSS were chosen from previous screening of antibiotics library (almost 450 drugs) (Uslu, et al., paper in prep.). MTT cell viability assays showed differential sensitivity to both compounds. AMX showed significant cytotoxicity with IC50 values of 91.364 ± 5.7 µM and 45.10 ± 8.2 µM in parental and resistant cells, respectively (Figure 3.3.1A). Notably, FSS showed strong effects with IC50 values of 111.5 ± 4.5 µM in parental cells and 57.5 ± 7.2 µM in resistant cells (Figure 3.3.1B). The increased sensitivity of resistant cells to both compounds suggests that they have the potential to address the metabolic vulnerabilities of chemoresistant phenotypes.

Colony formation tests, which often define metastatic potentials, also confirmed the long-term antiproliferative effects of both compounds. At IC50 concentrations, FSS reduced colony formation in resistant cells by 48.2% compared to 4.5% in parental cells, while AMX had even more pronounced effects, with a reduction of 66.9% and 8% in resistant and parental cells, respectively (Figure 3.3.1C). These results are consistent with previous studies indicating that targeting mitochondrial function can overcome chemoresistance by disrupting the altered metabolic pathways that support the survival of resistant cells (Guerra et al., 2017).

The increased efficiency of AMX and FSS in resistant cells demonstrates their potential as therapeutic options in combating chemoresistance. By exploiting the metabolic vulnerability of resistant cells, these antibiotics represent a promising approach to improving treatment responses in cancers resistant to conventional treatments.

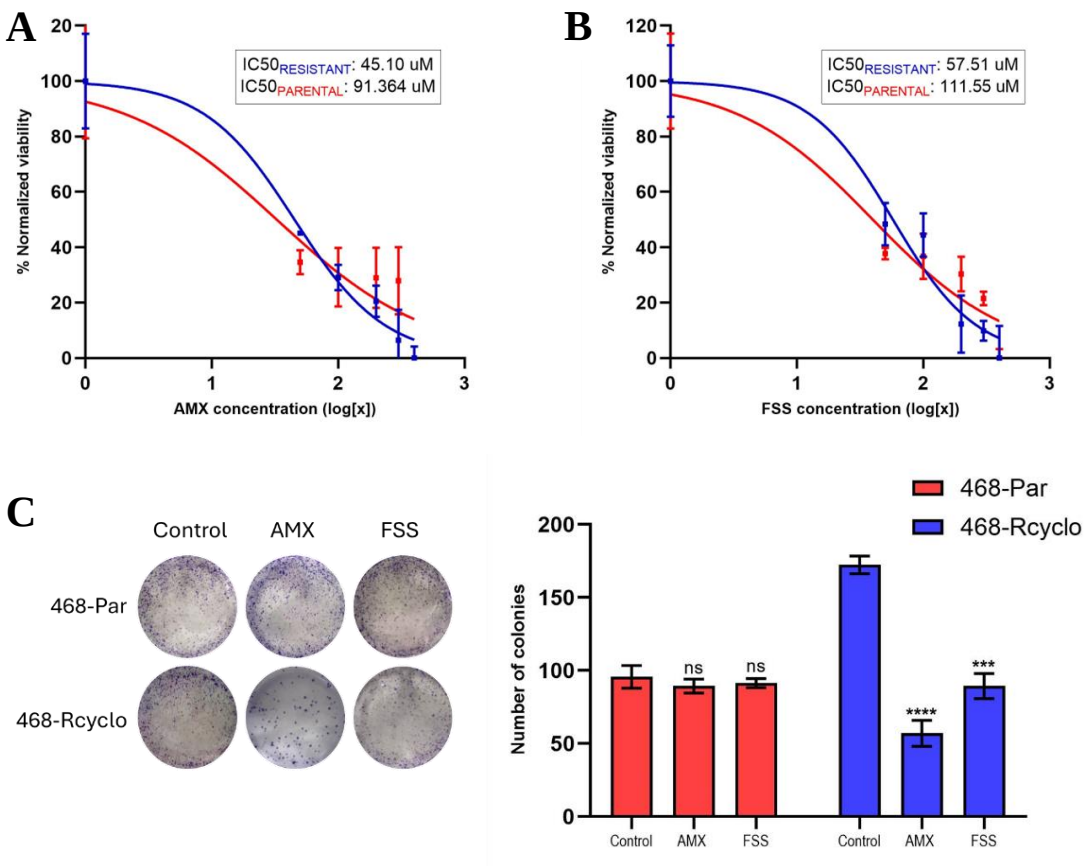

Figure 3.3.1: Drug-resistant cancer cells show sensitivity to antibiotics.

The viability differences of 468-Par and 468-Rcyclo in response to ***(A)*** AMX and ***(B)*** FSS were identified by MTT assay and the corresponding IC50 values for cyclophosphamide were calculated. ***(C)*** Colony formation assay was conducted to determine the profelirative ability of the cells when treated with AMX and FSS. 10^3 cells were incubated for 15 days and stained with 0.5% Crystal Violet solution. ImageJ was used to quantify the number of colonies. Statistical analyses were done, and graphs were prepared by using GraphPad Prism 10. Each value represents the mean ± SD of three replicates analyzed by Student t-test. *p<0.05, **p<0.01, ***p<0.001, ****p<0.0001, ns: non-significant.

3.4 Antibiotics Induce Mitochondrial Dysfunction in TNBC Cells

The impact on mitochondrial function was assessed through multiple approaches. In parental cells, AMX and FSS treatment did not show any significant effect in terms of mitochondrial complex II activity. However, both drugs significantly affected complex II activity in resistant cells, with AMX showing more potent inhibition. In resistant cells, AMX reduced Complex II activity by 54%, while FSS showed moderate inhibition of 12.4% (Figure 3.4.1A). These results suggest that resistant cells possess altered mitochondrial dynamics that make them more susceptible to the inhibitory effects of AMX and FSS.

Generation of ATP by mitochondrial complex V was used as another indicator of

mitochondrial function. ATP production was substantially impaired by both compounds, particularly in resistant cells. FSS treatment resulted in a 19.1% reduction in ATP levels in resistant cells compared to 17.9% in parental cells, while AMX caused 60.9% and 28.7% reduction in resistant and parental cells, respectively (Figure 3.4.1B). The greater sensitivity of resistant cells to these compounds suggests that they have the potential to target the enhanced mitochondrial function observed in the resistant phenotype.

To further investigate the impact of AMX and FSS on mitochondrial function, real-time analysis of cellular OCR was performed. The sequential addition of ADP, FCCP, and rotenone allowed the assessment of various parameters of mitochondrial respiration under different treatment conditions. OCR measurements demonstrated significant impairment of mitochondrial respiration by both compounds. AMX markedly reduced basal respiration, mitochondrial respiration, and maximal respiratory capacity in resistant cells, while FSS showed moderate effects (Figure 3.4.1D).

JC-1 staining revealed that both compounds effectively reduced mitochondrial membrane potential, with AMX showing more pronounced effects (3.4.1E-F). In parental cells, treatment with AMX at 70 μM resulted in a significant decrease in the fluorescence intensity ratio compared to control, indicating a reduction in mitochondrial membrane potential. This trend continued with 100 μM AMX, showing a more substantial decrease (Figure 3.4.1E). In resistant cells, the reduction in membrane potential was even more pronounced. Treatment with 50 μM AMX significantly decreased the red/green ratio, while 70 μM and 100 μM AMX resulted in highly significant reductions (Figure 3.5E). For parental cells, FSS treatment at concentrations of 30 μM, 90 μM, and 150 μM showed minimal changes in the fluorescence intensity ratio compared to the control, suggesting a marginal impact on mitochondrial membrane potential (Figure 3.4.1F). In contrast, resistant cells exhibited a more notable decrease in mitochondrial membrane potential. Treatment with 90 μM FSS led to a significant reduction in the red/green ratio and the effect was more pronounced at 150 μM FSS, where the ratio decreased significantly. Taken together, these results suggest that both AMX and FSS can effectively target mitochondrial function and thus exploit the metabolic vulnerabilities of chemoresistant cells.

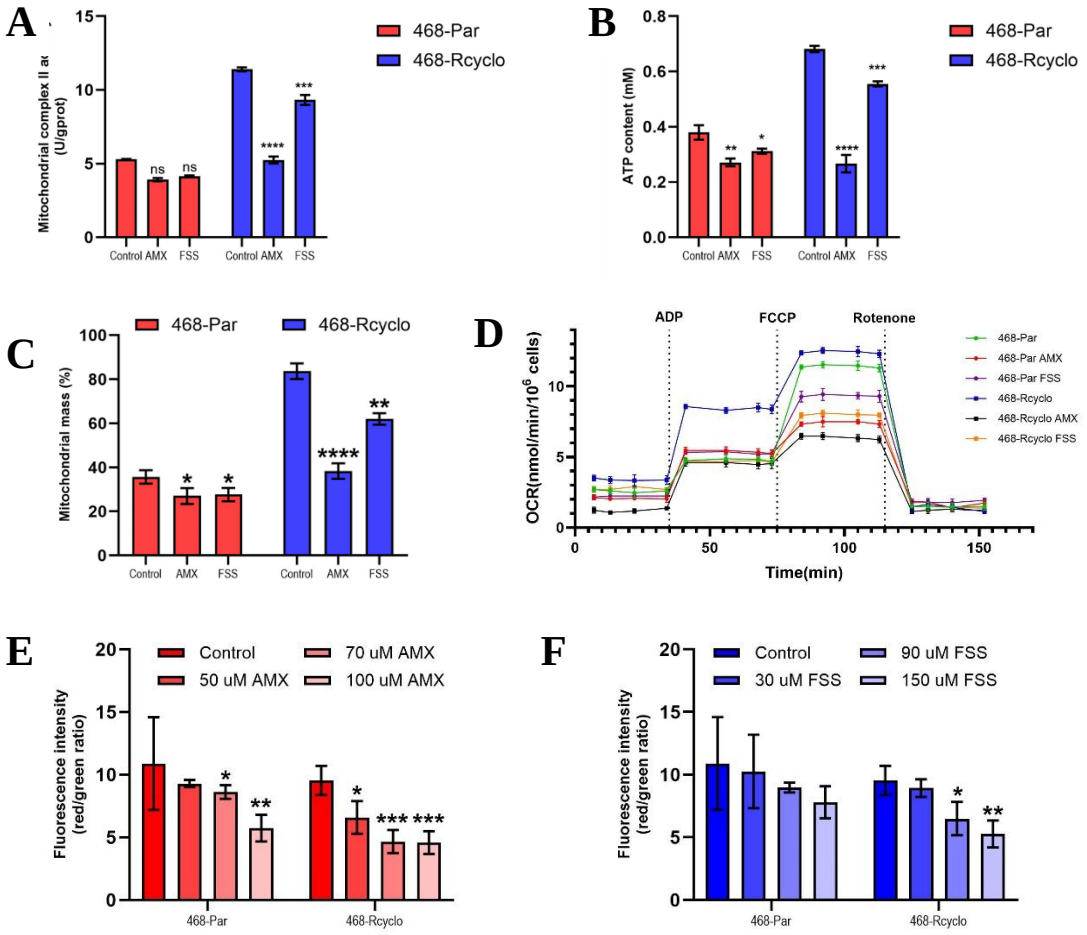

Figure 3.4.1: Antibiotics preferentially induce mitochondrial dysfunction in resistant cancer cells.

(A) The mitochondrial complex II activities of AMX- and FSS-treated 468-Par and 468-Rcyclo cells were done by calorimetric assays, according to the manufacturer's protocols. ***(B)*** The ATP content of AMX- and FSS-treated 468-Par and 468-Rcyclo cells was calculated by ATP calorimetric assay, according to the manufacturer's protocol. ***(C)*** The mitochondrial mass of the 468-Par and 468-Rcyclo cells was determined with MitoTracker Green FM dye. ***(D)*** The oxygen levels of AMX- and FSS-treated 468-Par and 468-Rcyclo cells were monitored with the sequential addition of ADP, FCCP, and rotenone. Changes in mitochondrial membrane potential of the 468-Par and 468-Rcyclo cells treated with AMX ***(E)*** and with FSS ***(F)*** were determined with JC-1 dye. Statistical analyses were done, and graphs were prepared by using GraphPad Prism 10. Each value represents the mean ± SD of three replicates analyzed by Student t-test. *p<0.05, **p<0.01, ***p<0.001, ****p<0.0001, ns: non-significant.

3.5 Antibiotics Target Stemness and Metastatic Behavior of Resistant TNBC Cells

The expression levels of Sox-2 and Nanog mRNA, key markers related to breast cancer stem cells and cancer cell progression, were assessed in both parental and resistant TNBC cells with/out AMX or FSS treatment (Figure 3.5.1A-B). In parental cells, Sox-2 mRNA expression was observed at baseline levels, which remained largely unchanged after treatment with AMX and FSS in both parental and resistant cells.

For Nanog mRNA expression, parental cells showed baseline values with minimal change

after AMX treatment. However, resistant cells showed significantly increased Nanog expression, indicating enriched stemness. AMX and FSS treatment significantly reduced Nanog expression in resistant cells, highlighting its ability to reduce these stem-like features. The analysis included MDA-MB-468-CSCs (468-CSC) as a positive control. These results suggest a possible therapeutic strategy to specifically reduce stem cell-like properties in resistant TNBC.

Next, the activities of MMPs in connection to the antiproliferative and antimetastatic roles of selected antibiotics were studied. These enzymes play a crucial role in the invasion and metastasis of cancer cells. To investigate the influence of AMX and FSS on MMP activity, gelatin zymography was performed to measure MMP-9 and MMP-2 activities in both parental and resistant TNBC cells. In parental cells, MMP-9 activity was significantly reduced by AMX treatment, while FSS had a minimal effect, with activity remaining almost unchanged compared to control. In resistant cells, AMX showed an even more significant reduction in MMP-9 activity, indicating a strong inhibition of invasive potential. FSS treatment also reduced MMP-9 activity, but to a lesser extent, suggesting partial efficacy and a possible limitation in its effectiveness in inhibiting invasion.

Similarly, MMP-2 activity showed a significant decrease upon AMX treatment in parental cells, whereas FSS did not significantly alter MMP-2 activity, reflecting its limited influence on MMP-9. In resistant cells, AMX significantly reduced MMP-2 activity, consistent with its effect on MMP-9 and supporting its potential antimetastatic effect. FSS treatment did not show a significant reduction in MMP-2 activity, indicating its specificity or limitation in targeting such enzyme pathways. The lack of significant changes in MMP-2 activity with FSS treatment suggests that AMX may have broader effects on enzymatic pathways relevant to metastasis. Overall, these results highlight the potential of AMX to not only target stemness properties in resistant TNBC cells but also inhibit MMP activity, suggesting a dual strategy to attenuate metastatic behavior in this aggressive cancer type.

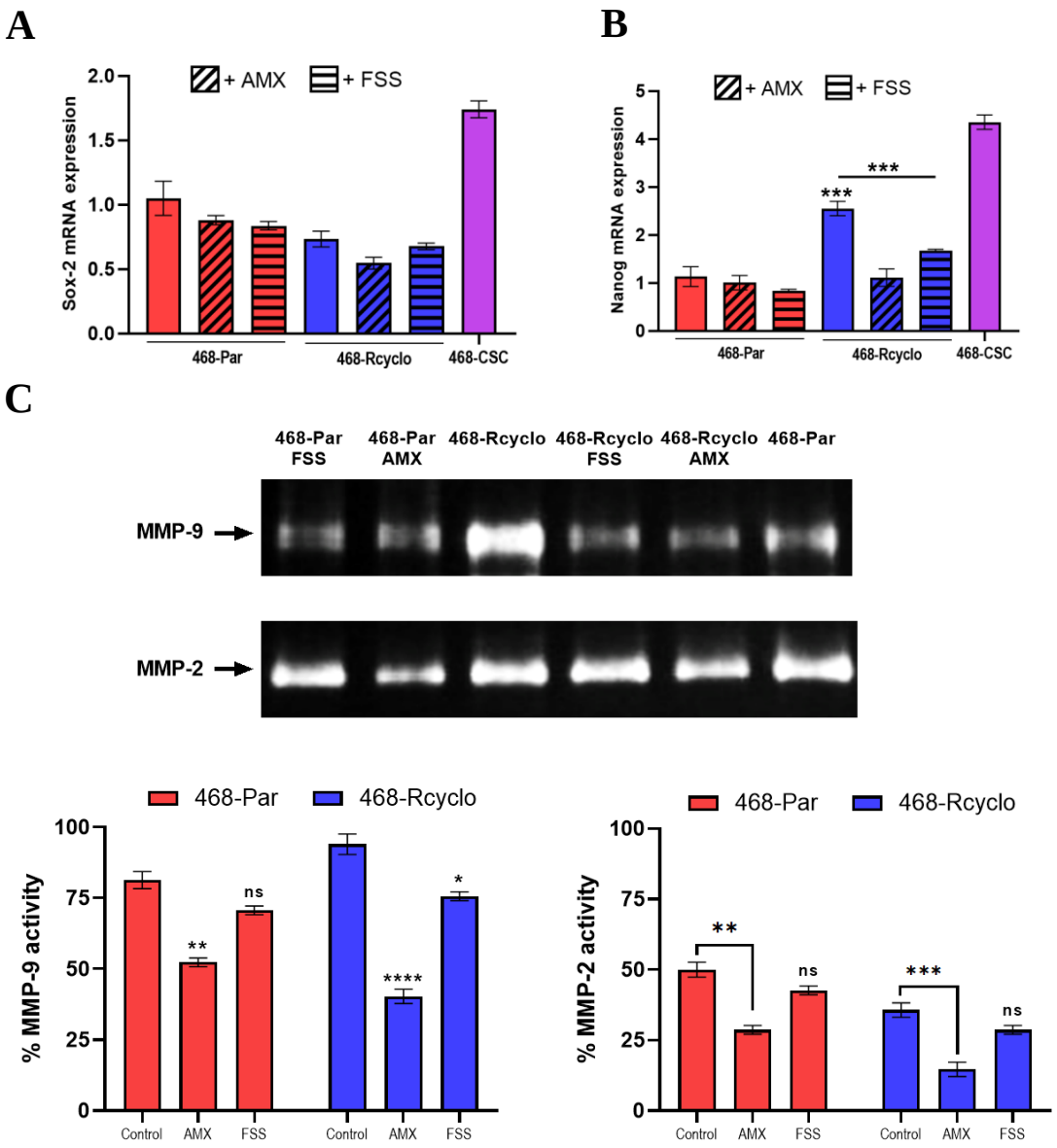

Figure 3.5.1: Antibiotics target stemness and metastatic behavior of resistant TNBC cells.

Cell pellets were collected, and total RNA was isolated and used for RT-qPCR to detect ***(A)*** Sox-2 and ***(B)*** Nanog mRNA expression. CSCs were used as a positive control. ***(C)*** Cell-free mediums were collected for performing gelatin zymography to measure the activity of MMP-9 and MMP-2. The white bands against a dark background indicate gelatinase activity. While MMP-9 is represented at ~92 kDa, MMP-2 is represented at ~72 kDa. Graphs were prepared by using Graphpad Prism 10. Each value represents the mean ± SD of three replicates analyzed by Student t-test. *p<0.05, **p<0.01, ***p<0.001, ****p<0.0001, ns: non-significant.

3.6 Complex II Protein Expression Is Upregulated in Chemotherapy-Resistant TNBT

To investigate mitochondrial protein expression levels in chemotherapy-sensitive and chemotherapy-resistant triple-negative breast tumors (TNBTs), Western blot analysis was

performed with antibodies detecting MT-CO1 (Complex IV), SDHB (Complex II), NDUFB8 (Complex I) and ATP5A (Complex V). Densitometric quantification of protein expression was normalized to VDAC for each sample (Figure 3.6.1).

MT-CO1, NDUFB8, and ATP5A protein levels were not significantly different between chemosensitive and chemoresistant TNBT samples, suggesting that mitochondrial complexes I, IV, and V protein levels are not associated with chemotherapy resistance. In contrast, SDHB expression was significantly higher in chemoresistant tumor samples compared to chemotherapy-sensitive samples. This upregulation indicates a potential role of mitochondrial complex II activity in developing chemotherapy resistance.

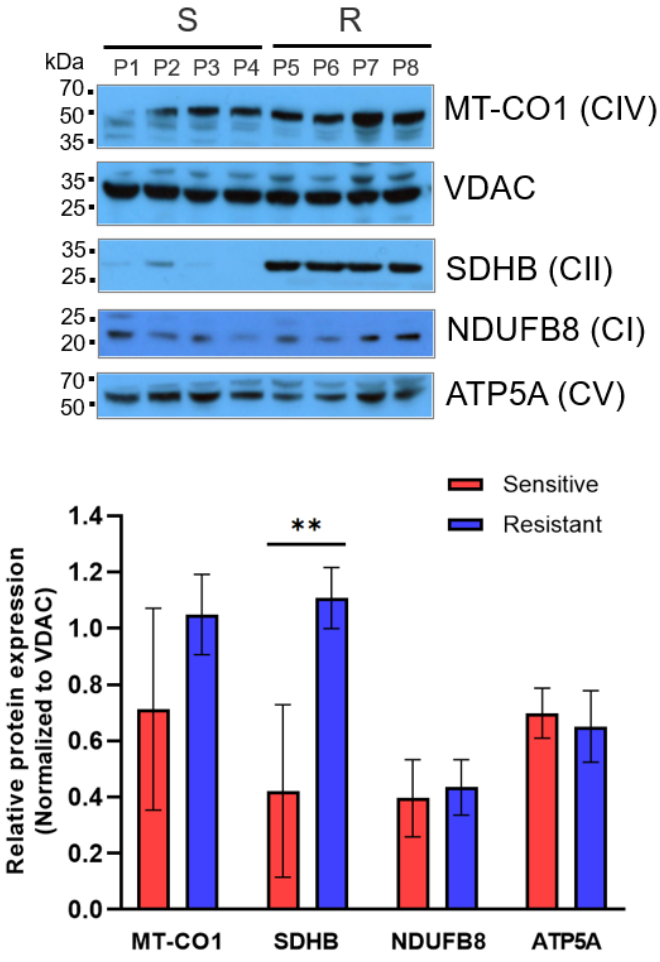

Figure 3.6.1: Mitochondrial complex II expression is upregulated in chemotherapy-resistant TNBT.

TNBT patient samples and minimal data annotation included in this study were provided by the Tumor Bank of Vall d'Hebron University Hospital Biobank (PT13/0010/), integrated in the Xarxa de Bancs de Tumors de Catalunya, and were processed following standard operating procedures with the appropriate approval of the Ethical and Scientific Committees. 8 of 12 samples were processed as they showed uniform distribution of cell mass with minimal fat content. Samples were homogenized with and lysed. After sonication on ice and centrifugation, supernatants were collected. Samples were normalized to total VDAC protein concentrations by Western blotting procedure. Graphs were prepared by using GraphPad Prism 10. Each value represents the mean ± SD of four replicates analyzed by Student t-test. *p<0.05, **p<0.01, ***p<0.001, ****p<0.0001, ns: non-significant.

3.7 Drug-Resistant TNBC Cells Show Sensitivity to TPP-linked Antibiotics

TPP-linked antibiotics (Figure 3.7.1) represent a second generation of antibiotics designed to enhance mitochondrial targeting. The inclusion of the TPP moiety significantly alters the pharmacokinetic properties of the antibiotic and allows selective accumulation in mitochondria due to the negative membrane potential of the organelle. This selective targeting is crucial for maximizing the therapeutic effects while minimizing systemic toxicity.

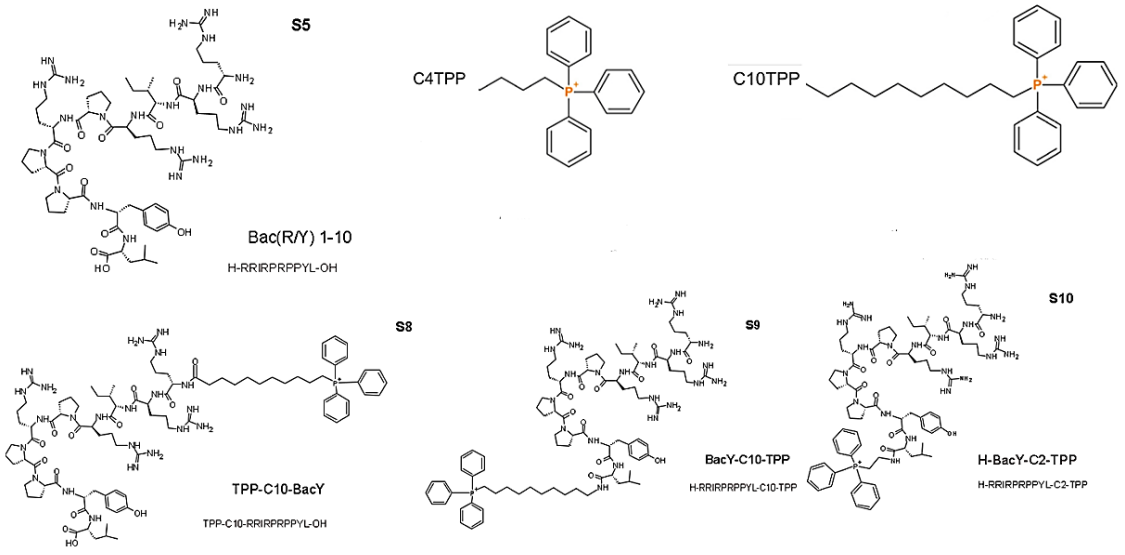

Figure 3.7.1: The TPP-linked drugs used in the study.
S5: Bacitracin. S8, S9, and S10: TPP-linked bacitracin with different configurations. C4-TPP and C10-TPP: TPP moieties not linked to any drug but only carbon atoms synthesized by our collaborators from Moscow State University.

To assess the efficacy of TPP-linked compounds as potential mitochondrial-targeting agents, we performed MTT cell viability assays on both parental and resistant TNBC cells. In parental cells, C4-TPP, S5, and S9 demonstrated significant cytotoxicity, with C4-TPP showing the lowest IC50 values, indicating potent inhibitory effects on cell survival. C10-TPP, S8, and S10 also reduced cell viability, with varying degrees of efficacy (Figure 3.7.2A).

In resistant cells, the trends shifted as all TPP-linked compounds displayed increased efficacy (Figure 3.7.2B). The resistant phenotype showed increased sensitivity, with C4-TPP, S5, S8, and S9 achieving the lowest IC50 values and thus the highest cytotoxicity. This increased sensitivity extended to other compounds as well, with C10-TPP and S10 showing markedly lower IC50 values compared to parental cells, highlighting their

potential to exploit vulnerabilities in the resistant phenotype (Figure 3.7.2C). These findings highlight the ability of TPP-linked compounds to target mitochondrial vulnerabilities, with the resistant TNBC cells demonstrating increased susceptibility.

Colony formation assays were conducted to evaluate the long-term effects of TPP-linked compounds on the proliferative capacity of both parental and resistant TNBC cells. In parental cells, treatment with TPP-linked compounds resulted in a reduction in colony numbers, although the effect was moderate across all compounds (Figure 3.7.2D). C4-TPP and S5 showed a noticeable decrease in colony formation compared to the control, indicating its potential in inhibiting cell proliferation. The other compounds, including C10-TPP, S8, S9, and S10, exhibited similar trends but with less pronounced effects.

Resistant cells demonstrated a more substantial response to TPP-linked compounds (Figure 3.7.2E). The resistant phenotype showed heightened sensitivity, with significant reductions in colony numbers observed for C4-TPP and S8. S5, C10-TPP, S9, and S10 also effectively reduced colony formation compared to the control, indicating their potential to impede the enhanced proliferative capabilities of resistant cells.

These results suggest that TPP-linked compounds are effective in targeting proliferative pathways, particularly in resistant TNBC cells, thereby revealing their potential as therapeutic agents to combat resistance by inhibiting cell growth and survival. The varying efficacy profiles suggest structure-dependent activities of these compounds, with some molecular configurations proving more effective at targeting cellular survival mechanisms. S8, a TPP-conjugated bacitracin derivative, demonstrated superior inhibitory effects on resistant cell growth and survival compared to its non-TPP counterpart, S5. This enhanced efficacy of the TPP-modified version aligns with previous research suggesting that TPP conjugation can improve targeted delivery to mitochondria, thereby increasing therapeutic efficacy (Sandoval-Acuña et al., 2016).

Notably, C4-TPP showed greater potency than some of the bacitracin-containing compounds, indicating that the TPP moiety alone possesses significant anticancer properties independent of antibiotic activity. The TPP moiety independently induces mitochondrial dysfunction through its inherent ability to accumulate in the mitochondria due to its lipophilic cationic properties. By taking advantage of the increased negative membrane potential characteristic of cancer cell mitochondria, TPP can selectively concentrate in these organelles at concentrations up to 1000-fold higher than in the cytoplasm, leading to disruption of mitochondrial function without the presence of any therapeutic agent (Murphy & Smith, 2007).

The superior effectiveness of C4-TPP compared to C10-TPP highlights the importance of carbon chain length in determining the effectiveness of the compound. The increased activity of the shorter carbon chain variant suggests that molecular size and lipophilicity play a critical role in the ability of the compounds to reach and influence mitochondrial targets.

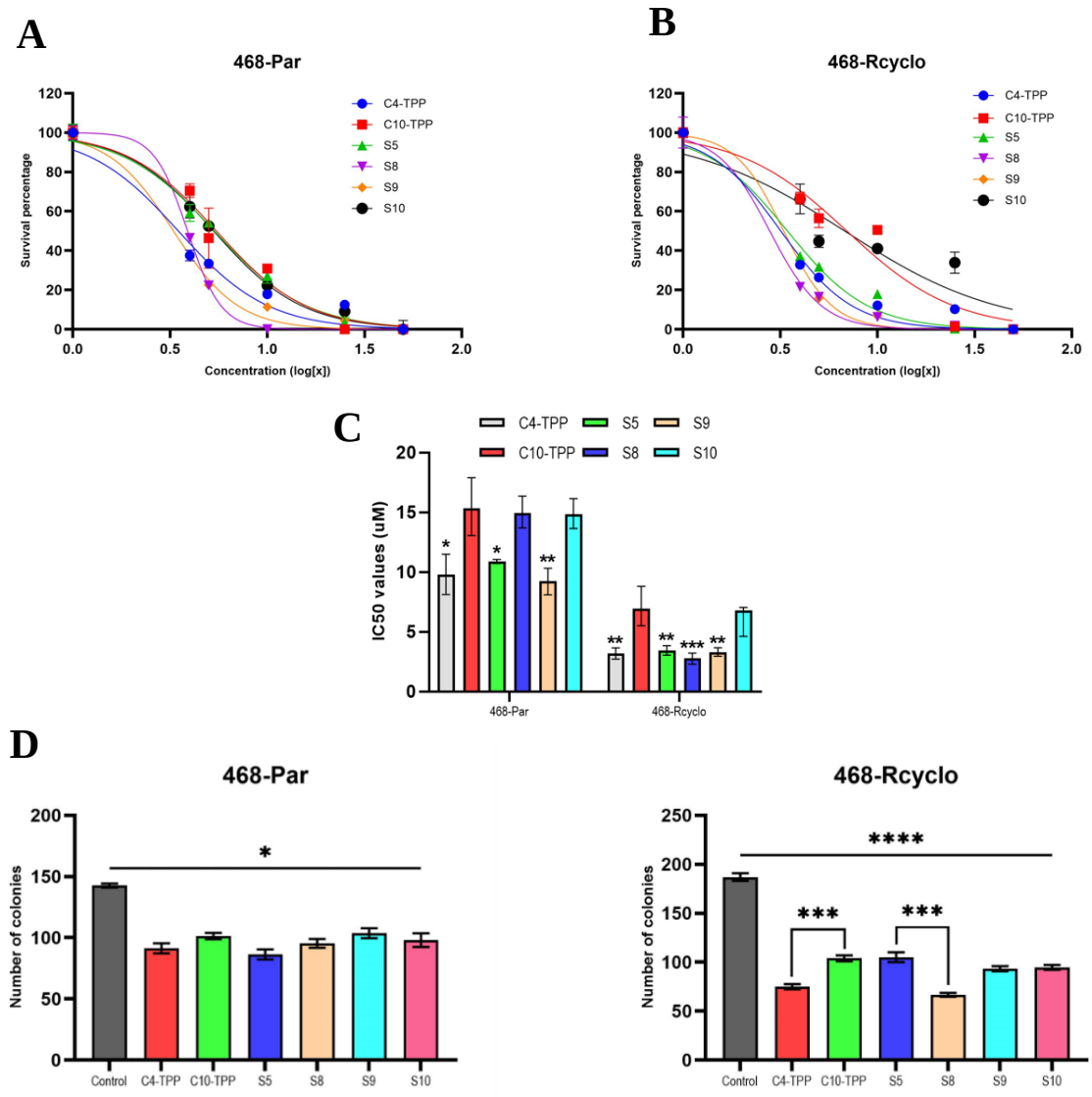

Figure 3.7.2: Drug-resistant TNBC cells show sensitivity to TPP-linked antibiotics.
The viability differences of ***(A)*** 468-Par and ***(B)*** 468-Rcyclo in response to TPP-linked antibiotics and TPP moieties were identified by MTT assay and ***(C)*** the corresponding IC50 values for cyclophosphamide were calculated. ***(D)*** Colony formation assay was conducted to determine the profelirative ability of the cells when treated with these drugs. 10^3 cells were incubated for 15 days and stained with 0.5% Crystal Violet solution. ImageJ was used to quantify the number of colonies. Statistical analyses were done, and graphs were prepared by using GraphPad Prism 10. Each value represents the mean ± SD of three replicates analyzed by Student t-test. *p<0.05, **p<0.01, ***p<0.001, ****p<0.0001, ns: non-significant.

3.8 TPP-linked Antibiotics Diminish Mitochondrial Function in TNBC Cells

The effects of TPP-linked compounds on mitochondrial mass, ATP content, and mitochondrial complex II activity were examined in both parental and resistant TNBC cells to assess their influence on cellular bioenergetics. In parental cells, treatment with TPP-bound compounds resulted in a small reduction in mitochondrial mass, with significant effects noted for all compounds (Figure 3.8.1A). This suggests a general influence on mitochondrial biogenesis or stability. Interestingly, ATP levels remained largely unchanged in the parental cells. (Figure 3.8.1B). Furthermore, complex II activity showed no significant changes, reflecting that they are not reliant on OXPHOS for energy production (Figure 3.8.1C).

On the other hand, resistant cells showed pronounced sensitivity to the TPP-bound compounds. Mitochondrial mass was significantly reduced for all compounds, with significant reductions observed for C4-TPP and S8, indicating marked changes in mitochondrial integrity or mitochondrial turnover (Figure 3.8.1A). Accordingly, ATP content was significantly reduced in resistant cells treated with these compounds, resulting in a significant reduction in cellular energy levels, highlighting their potential to disrupt metabolic functions that critically depend on mitochondrial ATP production (Figure 3.8.1B). Similarly, complex II activity showed significant decreases, particularly for C4-TPP and S8, highlighting the susceptibility of the respiratory chain to perturbations by these compounds (Figure 3.8.1C).

Overall, these results highlight the increased susceptibility of chemoresistant cells to mitochondrial disruption caused by TPP-bound compounds. The observed reduction in mitochondrial mass, ATP content, and complex II activity in resistant cells suggests that these compounds may effectively provide a potential therapeutic strategy to overcome drug resistance by impairing mitochondrial function.

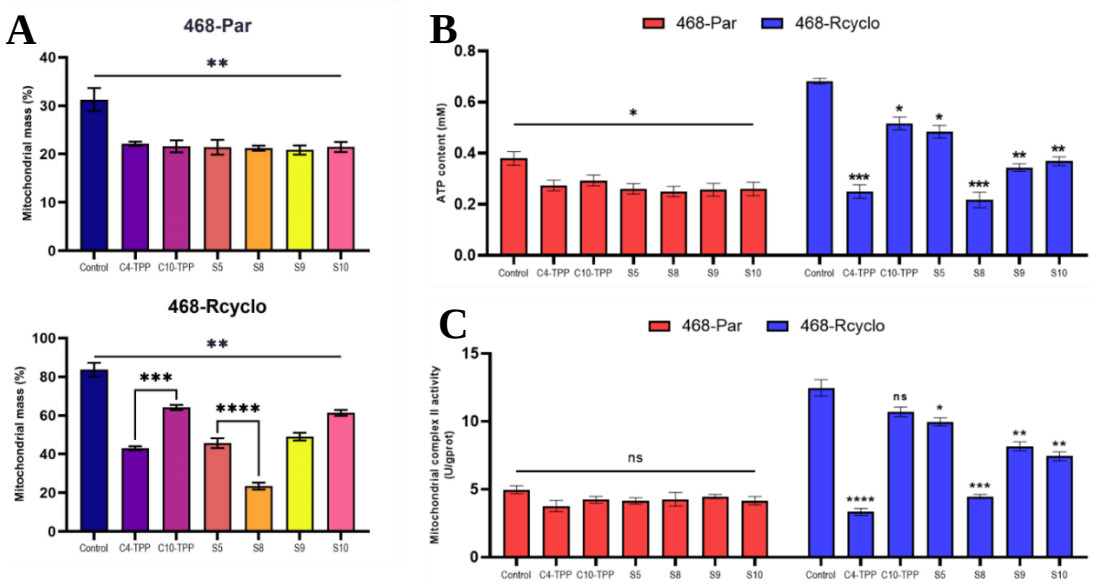

Figure 3.8.1: TPP-linked antibiotics diminish mitochondrial function in TNBC cells.

(A) The mitochondrial mass of the 468-Par and 468-Rcyclo cells treated with TPP-linked antibiotics and TPP moieties was determined with MitoTracker Green FM dye. ***(B)*** The ATP content of 468-Par and 468-Rcyclo cells treated with these drugs was calculated by ATP calorimetric assay, according to the manufacturer's protocol. ***(C)*** The mitochondrial complex II activities of 468-Par and 468-Rcyclo cells treated with these drugs were done by calorimetric assays, according to the manufacturer's protocols. Statistical analyses were done, and graphs were prepared by using GraphPad Prism 10. Each value represents the mean ± SD of three replicates analyzed by Student t-test. *p<0.05, **p<0.01, ***p<0.001, ****p<0.0001, ns: non-significant.

3.9 TPP-linked Antibiotics Reduce Metastatic Behavior of Resistant TNBC Cells

The influence of TPP-bound compounds on MMP activities, particularly MMP-9 and MMP-2, was examined in both resistant and parental TNBC cells using gelatin zymography (Figure 3.9.1). In resistant cells, treatment with TPP-bound compounds resulted in a significant reduction in MMP-9 activity. C4-TPP, C10-TPP, and S5 significantly reduced MMP-9 activity compared to controls, with S8 showing the greatest reduction (Figure 3.9.1A). This indicates the potential of these compounds to prevent invasive behavior by targeting the degradation of the extracellular matrix. MMP-2 activity in resistant cells also showed significant suppression, particularly at S8, S9, and S10, suggesting that these compounds effectively target MMP-related pathways, potentially reducing metastatic capability.

In parental cells, the effects of TPP-linked drugs were less pronounced, but still significant for certain compounds. More specifically, both S5 and S8 significantly reduced MMP-9 activity (Figure 3.9.1B). C4-TPP showed moderate inhibition of MMP-2 in parental cells, highlighting its broader effect on all cell types and its potential to

impair matrix remodeling.

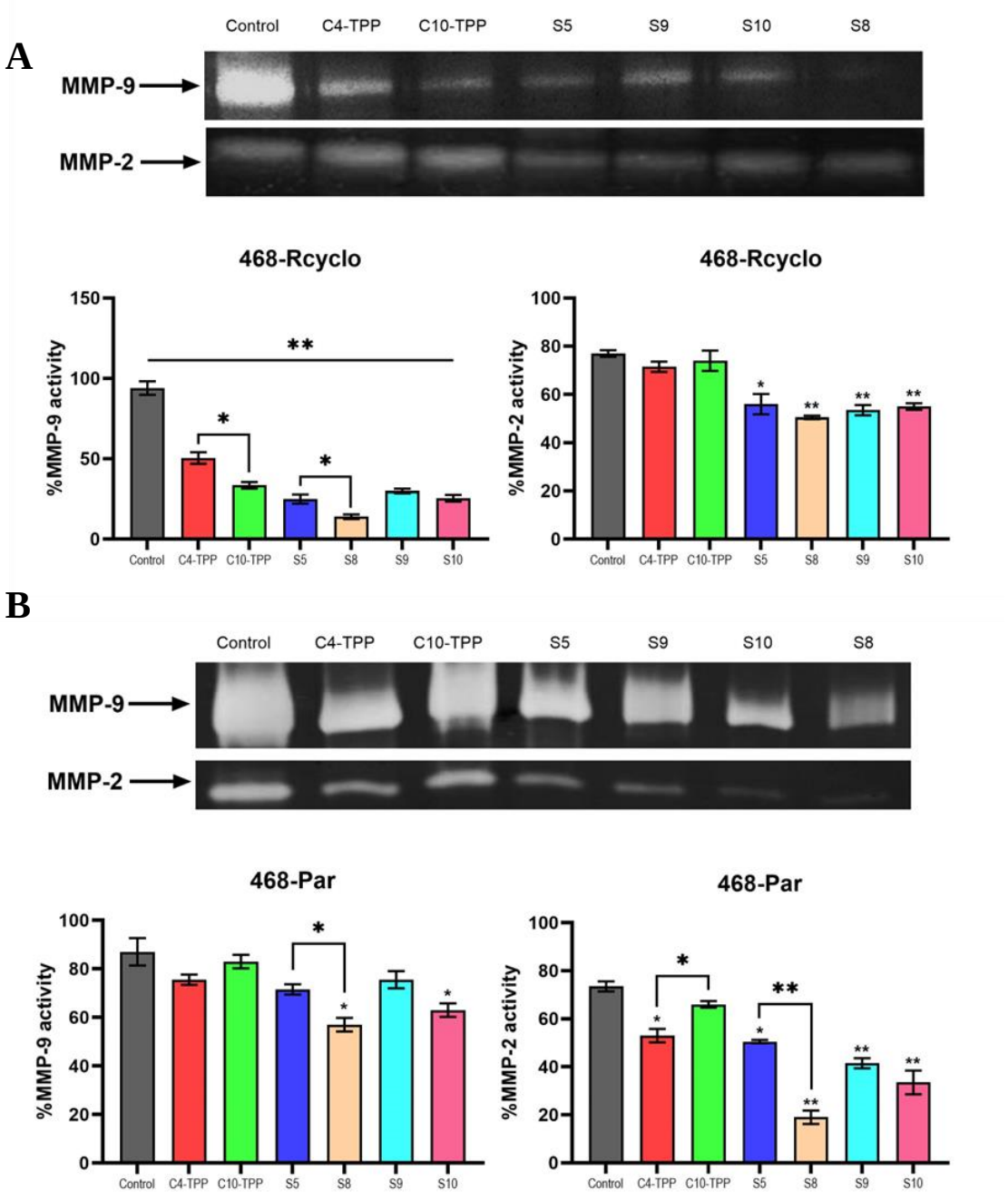

Figure 3.9.1: TPP-linked antibiotics reduce metastatic behavior of resistant TNBC cells by decreasing activity of MMPs.

Cell-free mediums were collected for performing gelatin zymography to measure the activity of MMP-9 and MMP-2 in **(A)** parental and **(B)** resistant TNBC cells in response to TPP-linked antibiotics and TPP moieties. The white bands against a dark background indicate gelatinase activity. While MMP-9 is represented at ~92 kDa, MMP-2 is represented at ~72 kDa. Graphs were prepared by using Graphpad Prism 10. Each value represents the mean ± SD of two replicates analyzed by Student t-test. *p<0.05, **p<0.01, ***p<0.001, ****p<0.0001, ns: non-significant.

These results highlight the ability of TPP-bound compounds to selectively impair MMP activities, particularly in resistant TNBC cells. The pronounced reduction in MMP

activities suggests the potential of these compounds to inhibit metastasis and provides a viable strategy to target resistant cancer cells by attenuating their invasive potential.

3.10 Combination of Cyclophosphamide with Antibiotics Additively Decreases The Viability of TNBC Cells

Having different mutations and activated pathways, drug-resistant cells often develop vulnerabilities that can be exploited through combination strategies. Therefore, combinatorial treatment of the anti-cancer drug cyclophosphamide with antibiotics AMX, FSS, and TPP-linked bacitracin could be more effective than either treatment alone. When cell viability was examined across different treatments, parental cells showed a consistent response, with most treatments not significantly altering viability compared to the control (Figure 3.10.1A). Remarkably, treatments such as different concentrations of AMX or FSS in combination with IC40-cyclophosphamide did not result in statistically significant differences, suggesting that these cells retained viability under these conditions. In contrast, the resistant cells showed different responses (Figure 3.10.1B).

Treatment with IC15 AMX in combination with IC40 cyclophosphamide slightly but not significantly reduced viability. However, combinations of IC20-40 AMX and IC20-40 FSS with IC40-cyclophosphamide resulted in combinatorial effects and showed a significant decrease in cell viability. The most significant reductions were observed for IC30-40 AMX and IC40 FSS in combination with IC40-cyclophosphamide, resulting in a significant reduction in viability.

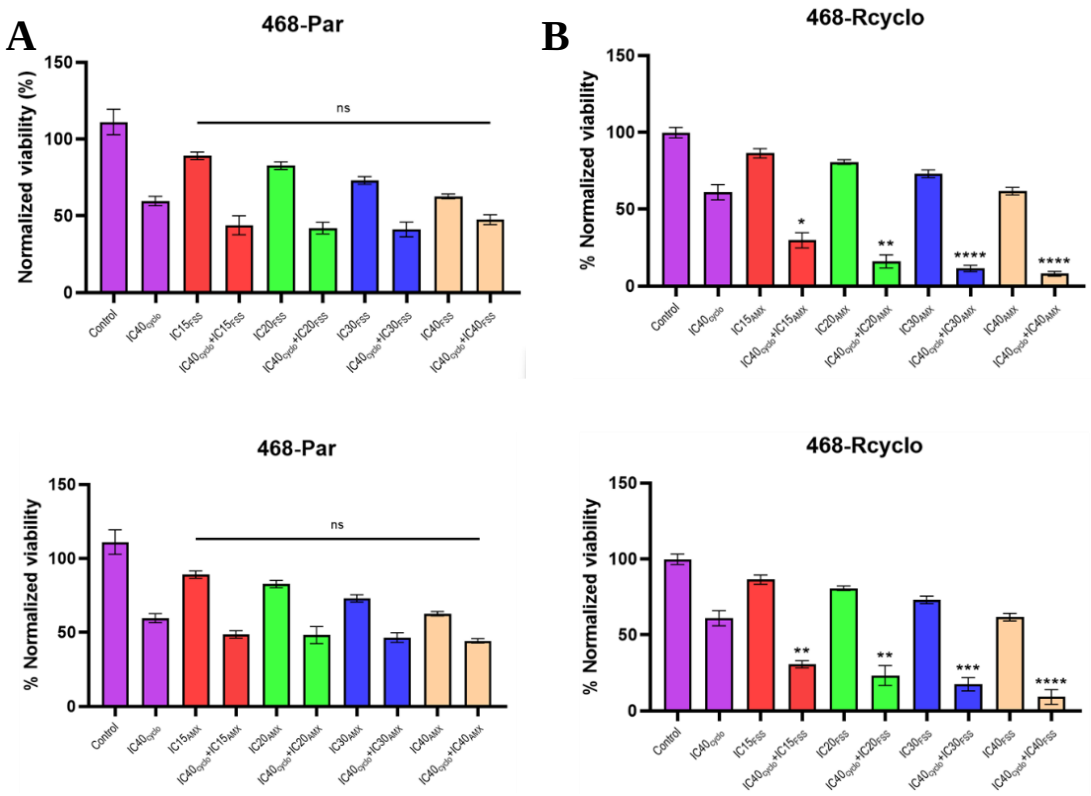

Figure 3.10.1: Combination of cyclophosphamide with AMX and FSS additively reduces the viability of TNBC cells.

The viability differences of ***(A)*** 468-Par and ***(B)*** 468-Rcyclo in response to the combination of IC40 cyclophosphamide with several concentrations of AMX and FSS were identified by MTT assay. Graphs were prepared by using Graphpad Prism 10. Each value represents the mean ± SD of two replicates analyzed by Student t-test. *p<0.05, **p<0.01, ***p<0.001, ****p<0.0001, ns: non-significant.

Combinatorial treatment was also conducted for TPP-linked bacitracin (S8) and C4-TPP and it was observed that the resistant cells revealed notable changes (Figure 3.10.2B). The combination of IC40 cyclophosphamide with IC20-40 S8 led to a significant reduction in viability, indicating a strong synergistic effect and emphasizing the potency of these combinations. However, the combination of IC40 cyclophosphamide with various concentrations of C4-TPP did not show any significant effects.

In contrast, the parental cells showed a consistent response across treatments, with no significant changes in viability, regardless of whether S8 or C4-TPP with cyclophosphamide (Figure 3.10.2A). This suggests that parental cells are less susceptible to combinatorial treatment strategies compared to resistant cells.

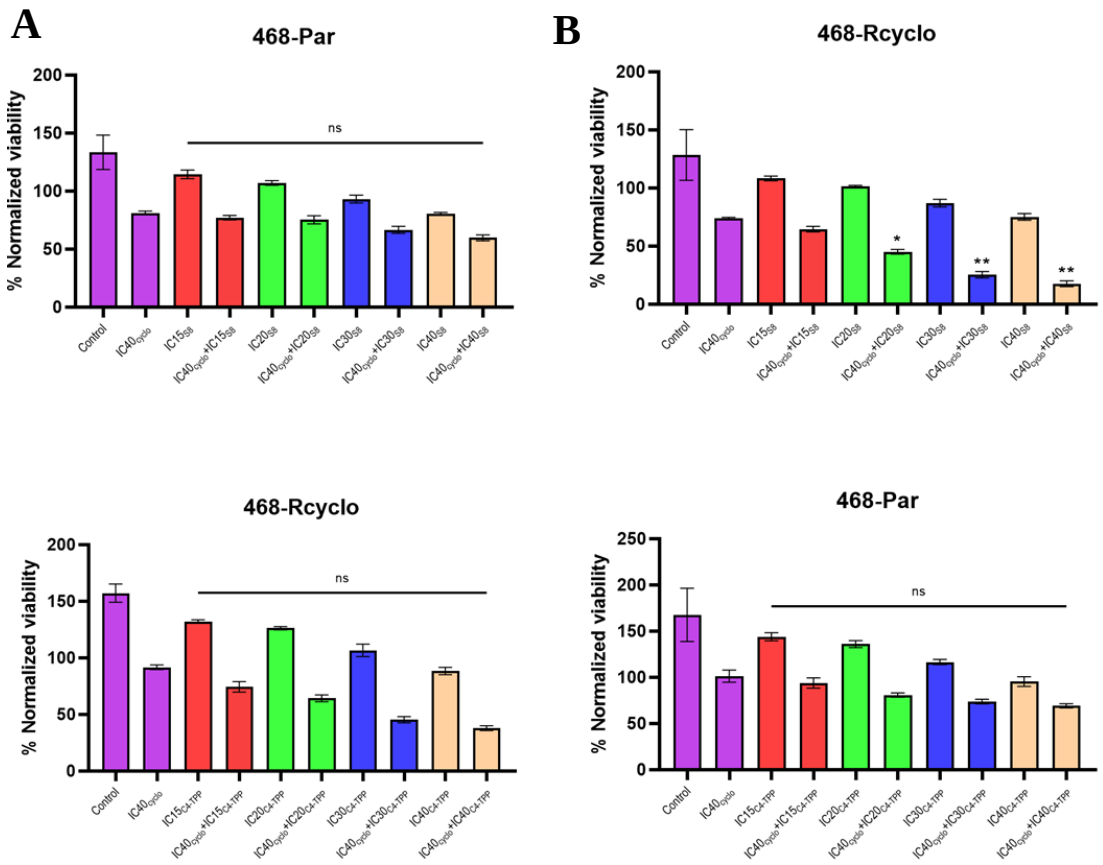

Figure 3.10.2: Combination of cyclophosphamide with TPP-linked bacitracin (S8) additively reduces the viability of TNBC cells.

The viability differences of ***(A)*** 468-Par and ***(B)*** 468-Rcyclo in response to the combination of IC40 cyclophosphamide with several concentrations of S8 and C4-TPP were identified by MTT assay. Graphs were prepared by using Graphpad Prism 10. Each value represents the mean ± SD of two replicates analyzed by Student t-test. *p<0.05, **p<0.01, ***p<0.001, ****p<0.0001, ns: non-significant.

3.11 Antibiotics Reduce Tumor Growth in Chemoresistant TNBC

Often, the results of *in vivo* experiments cannot be translated into clinics. To this end, animal work should be performed. To see the effects of selected MDF-inducing antibiotics on TNBC tumor growth, an *in vivo* study was carried out (Figure 3.11.1). The *in vivo* study examined tumor growth in mice injected with 468-Par and 468-Rcyclo cells in untreated (control) and AMX-treated groups over a six-week period. Both cell lines initially showed similar tumor growth rates. However, by the third week, the untreated resistant cells showed a significant increase in tumor volume compared to the untreated parental cells, suggesting higher tumorigenic potential and further highlighting the challenges associated with treating resistant TNBC.

AMX treatment, provided to mice in drinking water, had a significant effect on limiting

tumor growth in resistant cells. In the AMX-treated resistant tumors, the volume remained consistently lower than in the untreated group of animals throughout the study. The sustained suppression of tumor growth in resistant cells treated with AMX suggests that this compound may effectively target the unique vulnerabilities of chemoresistant tumors, possibly through mechanisms demonstrated in this study. However, AMX treatment did not show any significant effect on tumor volume for parental cells, indicating a selective action of the drug on resistant phenotype.

Overall, these results reveal that AMX may reduce the growth of tumors derived from resistant TNBC cells, suggesting that AMX may serve as a valuable therapeutic option to combat chemoresistant TNBC tumors.

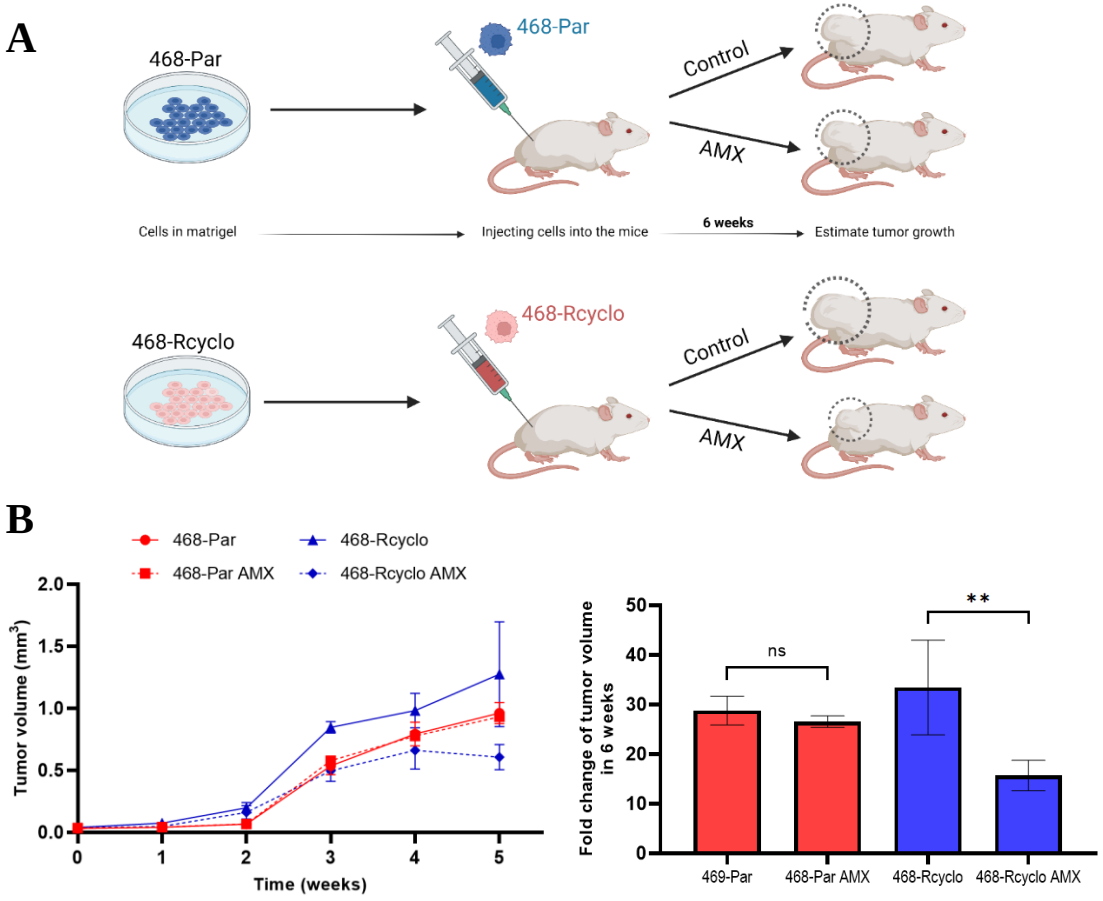

Figure 3.11.1: AMX specifically reduces TNBT growth derived from chemoresistant TNBC cells.

(A) 24 mice were divided into two groups: one injected with parental cells and the other injected with resistant cells. After the injection, the mice were housed with free access to water and food. Ten days later, based on their tumor volumes, the mice were randomized into four groups containing 6 mice each: control groups of 468-Par and 468-Rcyclo mice and experimental groups of 468-Par and 468-Rcyclo mice treated with AMX in drinking water once a week. ***(B)*** Tumor dimensions were measured weekly with three readings per mouse for accuracy. Tumor volume was calculated using the formula: Tumor Volume (mm^3) = (X × Y × Z) / 2. Graphs were prepared by using Graphpad Prism 10. Each value represents the mean ± SD of two replicates analyzed by Student t-test. *p<0.05, **p<0.01, ***p<0.001, ****p<0.0001, ns: non-significant.

To assess the efficacy of AMX treatment in reducing tumor growth induced by CSCs, 468-CSC tumor cells were injected into mice, and tumor volume was monitored over time (Figure 3.11.2). In the untreated group, tumor volume demonstrated a continuous and significant increase over the course of 7 weeks, reaching approximately 1.5 mm^3 by the endpoint. In contrast, the group treated with AMX exhibited significantly attenuated tumor growth, with tumor volumes remaining substantially lower throughout the study period.

Quantitative analysis of the fold change in tumor volume confirmed that AMX treatment markedly reduced tumor growth. At 7 weeks, the fold change in tumor volume was significantly lower in the AMX-treated group compared to the untreated group. The data demonstrate that AMX effectively suppresses tumor growth in the 468-CSC tumor model, suggesting its potential therapeutic utility in targeting cancer stem cell-driven tumor progression. AMX treatment led to a significant reduction in both tumor volume and growth rate, highlighting its potent antitumor effects.

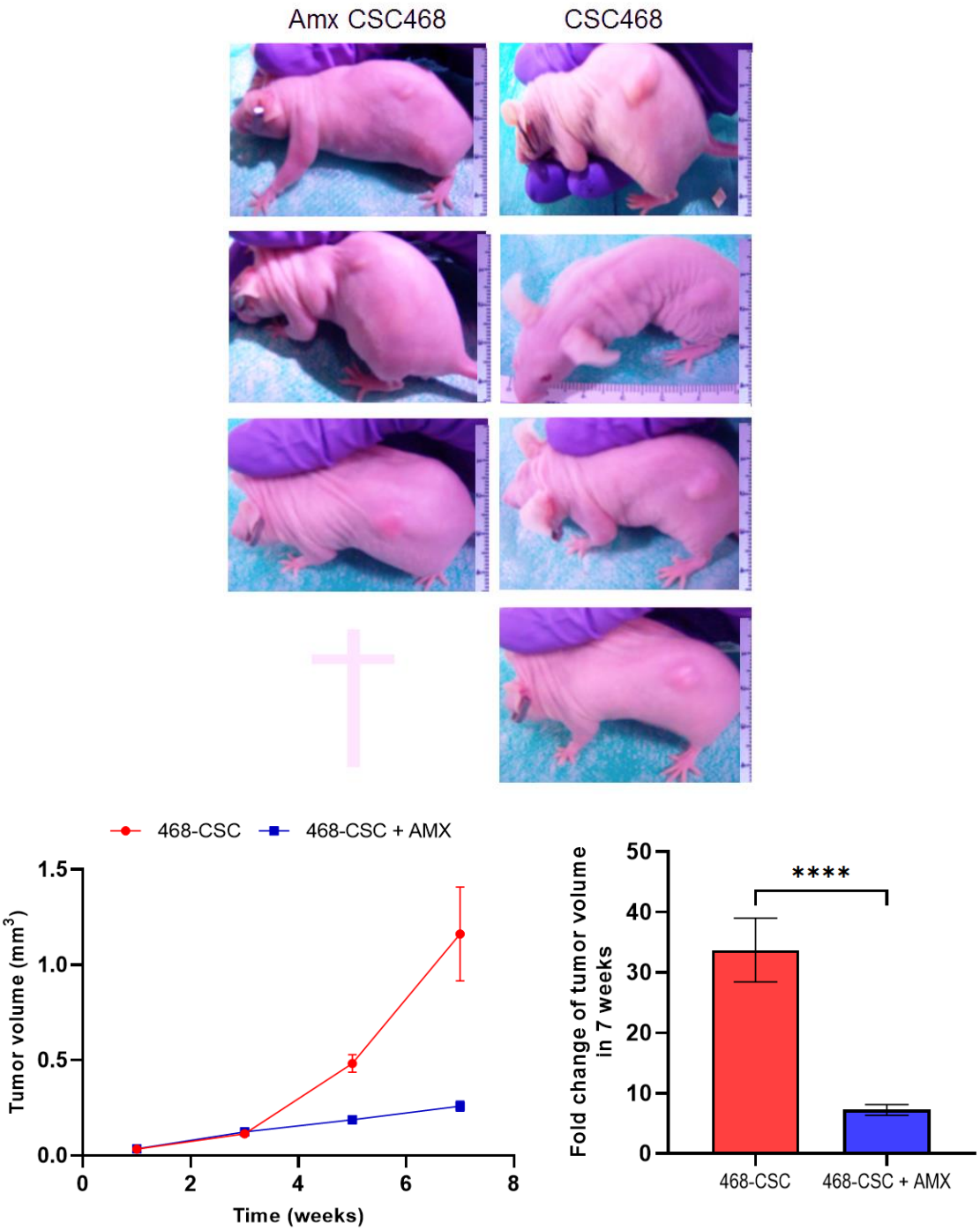

Figure 3.11.2: AMX reduces the growth of tumors derived from CSCs.

8 mice were injected with CSC and after the injection, the mice were housed with free access to water and food. Ten days later, based on their tumor volumes, the mice were randomized into two groups containing 4 mice each: the control group of 468-CSC mice and the experimental group of 468-CSC mice treated with AMX in drinking water once a week. Tumor dimensions were measured weekly with three readings per mouse for accuracy. Tumor volume was calculated using the formula: Tumor Volume (mm^3) = (X × Y × Z) / 2. Graphs were prepared by using Graphpad Prism 10. Each value represents the mean ± SD of two replicates analyzed by Student t-test. *p<0.05, **p<0.01, ***p<0.001, ****p<0.0001, ns: non-significant.

4. DISCUSSION

Drug resistance in TNBC remains a major therapeutic challenge that calls for innovative strategies to overcome treatment resistance. This study provides strong evidence that antibiotics and their TPP-conjugated derivatives can be used to target chemoresistant TNBC through multiple mechanisms. The results show that antibiotics and TPP-linked compounds effectively disrupt mitochondrial function, particularly in resistant TNBC cells (Figure 3.4.1 & Figure 3.8.1). The significant decrease in mitochondrial mass, ATP content, and complex II activity in resistant cells suggests their increased dependency on mitochondrial function for survival. This aligns with the concept of bioenergetic vulnerability of resistant cancer cells, where adaptation to chemotherapy may lead to increased reliance on OXPHOS.

The greater efficacy of TPP-conjugated compounds emphasizes how crucial molecular design is for mitochondrial targeting. These substances have a selective mechanism to destroy cancer cells and potentially avoid damage to healthy tissue because they can accumulate in the mitochondria up to 1000 times greater than cytoplasmic concentrations, therefore reducing overall toxicity for the body. A significant finding of this study is the ability of antibiotics to target cancer stem cell-like properties in resistant TNBC. The reduction in Sox-2 and Nanog expression following AMX treatment specifically in resistant cells suggests that these compounds can effectively target the stem cell population that often drives resistance and recurrence (Figure 3.5.1A-B). This is particularly important as cancer stem cells are typically resistant to conventional chemotherapy and likely to be responsible for metastasis.

In addition, the pronounced effects on MMP-9 and MMP-2 activities, especially in resistant cells treated with TPP-linked compounds, also demonstrate their potential in preventing metastasis (Figure 3.5.1C) and therefore disease progression in aggressive TNBC cases.

Among the analyzed mitochondrial proteins, only SDHB demonstrated a statistically significant increase in expression in chemotherapy-resistant tumor samples (Figure 3.6.1). These results implicate complex II as a potential contributor to altered metabolic processes in chemotherapy-resistant tumors, while other complexes remain unchanged at the protein expression level. These results align well with the increased activity of mitochondrial complex II determined previously (Figure 3.2.1).

The combination studies with cyclophosphamide showed promising synergistic effects, especially on resistant cells. The increased potency of AMX and TPP-bound bacitracin (S8) in combination with cyclophosphamide suggests a potential strategy to overcome drug resistance through targeted approaches (Figure 3.10.1 & Figure 3.10.2). This synergy could enable lower doses of conventional chemotherapy while maintaining therapeutic efficacy.

Finally, the *in vivo* studies provided crucial confirmation of the in vitro results and demonstrated that AMX effectively suppresses tumor growth, particularly in resistant TNBC models (Figure 3.11.1). This selective effect against resistant tumors while sparing the parental cells suggests a therapeutic window that could be used clinically.

The effectiveness of antibiotics against chemoresistant TNBC can be attributed to several interrelated mechanisms. First and foremost, it is crucial that they target mitochondrial function, in particular OXPHOS. The increased accumulation of TPP compounds in the mitochondria destabilizes the integrity of the organelle, thereby disrupting the bioenergetics that are essential for cancer cell survival. This disruption of mitochondria results in decreased ATP production, which supports energy-dependent processes critical to chemoresistant tumor growth and metastasis. Resistance is often accompanied by a greater reliance on mitochondrial metabolism, creating a significant vulnerability that can be exploited by antibiotic treatment.

In addition, these antibiotics can influence important signaling pathways that are associated with the development and differentiation of cancers. By reducing levels of stem cell markers such as Sox-2 and Nanog, these compounds could shift the balance from a proliferative state of cancer stem cells to a more differentiated and less aggressive phenotype. This transition not only reduces the ability of tumors to self-renew and spread, but also sensitizes the cells to other therapeutic modalities.

The anti-metastatic effects induced by the antibiotics are likely mediated through the inhibition of MMP-9 and MMP-2, which are crucial for extracellular matrix remodeling and invasive potential. By targeting these signaling pathways, the antibiotics

not only prevent the invasive behavior of cancer cells but also potentially normalize the tumor microenvironment, making it less conducive to metastasis.

In conclusion, this study highlights the potential of selected antibiotics and their TPP-linked derivatives as promising therapeutics against chemoresistant TNBC. Their multifunctional effects - in particular the impairment of mitochondrial OXPHOS, the targeted combating of cancer strains, and the inhibition of metastasis pathways - underline their ability to significantly alter the course of therapy-resistant tumors.

Future investigations should focus on optimizing these compounds for improved efficacy and further exploring their mechanisms in combination therapies. Clinical trials evaluating the safety and efficacy of these antibiotics in TNBC patients, particularly those with a chemoresistant phenotype, will be crucial to translating these preclinical findings into concrete therapeutic protocols. Additionally, understanding the molecular basis of the interactions across antibiotics that inhibit OXPHOS and cancer cell microenvironment could pave the way for personalized treatment approaches and ultimately improve outcomes for patients battling this aggressive form of breast cancer. Further research to optimize dosing regimens and explore potential synergistic effects with existing chemotherapeutic agents will be critical to developing robust treatment protocols for chemoresistant TNBC.

5. REFERENCES

Abad, E., García-Mayea, Y., Mir, C., Sebastian, D., Zorzano, A., Potesil, D., Zdrahal, Z., Lyakhovich, A., & Lleonart, M. E. (2019). Common metabolic pathways implicated in resistance to chemotherapy point to a key mitochondrial role in breast cancer. *Molecular and Cellular Proteomics*, *18*(2), 231–244. https://doi.org/10.1074/mcp.RA118.001102

Ahlmann, M., & Hempel, G. (2016). The effect of cyclophosphamide on the immune system: implications for clinical cancer therapy. *Cancer Chemotherapy and Pharmacology*, *78*(4), 661–671. https://doi.org/10.1007/S00280-016-3152-1/FIGURES/2

Akhunzianov, A. A., Nesterova, A. I., Wanrooij, S., Filina, Y. V., Rizvanov, A. A., & Miftakhova, R. R. (2023). Unravelling the Therapeutic Potential of Antibiotics in Hypoxia in a Breast Cancer MCF-7 Cell Line Model. *International Journal of Molecular Sciences*, *24*(14), 11540. https://doi.org/10.3390/IJMS241411540/S1

Almansour, N. M. (2022). Triple-Negative Breast Cancer: A Brief Review About Epidemiology, Risk Factors, Signaling Pathways, Treatment and Role of Artificial Intelligence. *Frontiers in Molecular Biosciences*, *9*, 836417. https://doi.org/10.3389/FMOLB.2022.836417

Amaravadi, R. K., Kimmelman, A. C., & Debnath, J. (2019). Targeting Autophagy in Cancer: Recent Advances and Future Directions. *Cancer Discovery*, *9*(9), 1167. https://doi.org/10.1158/2159-8290.CD-19-0292

Ashton, T. M., Gillies McKenna, W., Kunz-Schughart, L. A., & Higgins, G. S. (2018). Oxidative phosphorylation as an emerging target in cancer therapy. *Clinical Cancer Research*, *24*(11), 2482–2490. https://doi.org/10.1158/1078-0432.CCR-17-3070/274584/AM/OXIDATIVE-PHOSPHORYLATION-AS-AN-EMERGING-TARGET-IN

Batlle, E., & Clevers, H. (2017). Cancer stem cells revisited. *Nature Medicine 2017 23:10*, *23*(10), 1124–1134. https://doi.org/10.1038/nm.4409

Battogtokh, G., Choi, Y. S., Kang, D. S., Park, S. J., Shim, M. S., Huh, K. M., Cho, Y. Y., Lee, J. Y., Lee, H. S., & Kang, H. C. (2018). Mitochondria-targeting drug conjugates for cytotoxic, anti-oxidizing and sensing purposes: current strategies and future perspectives. *Acta Pharmaceutica Sinica B*, *8*(6), 862–880. https://doi.org/10.1016/J.APSB.2018.05.006

Bertos, N. R., & Park, M. (2011). Breast cancer — one term, many entities? *The Journal of Clinical Investigation*, *121*(10), 3789–3796. https://doi.org/10.1172/JCI57100

Bharti, A. C., & Aggarwal, B. B. (2002). Chemopreventive Agents Induce Suppression of Nuclear Factor-κB Leading to Chemosensitization. *Annals of the New York Academy of Sciences*, *973*(1), 392–395. https://doi.org/10.1111/J.1749-6632.2002.TB04671.X

Birsoy, K., Wang, T., Chen, W. W., Freinkman, E., Abu-Remaileh, M., & Sabatini, D. M. (2015). An Essential Role of the Mitochondrial Electron Transport Chain in Cell Proliferation Is to Enable Aspartate Synthesis. *Cell*, *162*(3), 540–551. https://doi.org/10.1016/J.CELL.2015.07.016

Bokil, A., & Sancho, P. (2019). Mitochondrial determinants of chemoresistance. *Cancer Drug Resistance*, *2*(3), 634–646. https://doi.org/10.20517/cdr.2019.46

Bray, F., Laversanne, M., Sung, H., Ferlay, J., Siegel, R. L., Soerjomataram, I., & Jemal, A. (2024). Global cancer statistics 2022: GLOBOCAN estimates of incidence and mortality worldwide for 36 cancers in 185 countries. *CA: A Cancer Journal for Clinicians*, *74*(3), 229–263. https://doi.org/10.3322/CAAC.21834

Bray, F., Laversanne, M., Weiderpass, E., & Soerjomataram, I. (2021). The ever-increasing importance of cancer as a leading cause of premature death worldwide. *Cancer*, *127*(16), 3029–3030. https://doi.org/10.1002/CNCR.33587

Cadassou, O., & Jordheim, L. P. (2023). OXPHOS inhibitors, metabolism and targeted therapies in cancer. *Biochemical Pharmacology*, *211*, 115531. https://doi.org/10.1016/J.BCP.2023.115531

Caino, M. C., Ghosh, J. C., Chae, Y. C., Vaira, V., Rivadeneira, D. B., Faversani, A., Rampini, P., Kossenkov, A. V., Aird, K. M., Zhang, R., Webster, M. R., Weeraratna, A. T., Bosari, S., Languino, L. R., & Altieri, D. C. (2015). PI3K therapy reprograms mitochondrial trafficking to fuel tumor cell invasion.

Proceedings of the National Academy of Sciences of the United States of America, *112*(28), 8638–8643. https://doi.org/10.1073/pnas.1500722112

Cancer Statistics - NCI. (2024). https://www.cancer.gov/about-cancer/understanding/statistics

Carvalho, L. S., Gonçalves, N., Fonseca, N. A., & Moreira, J. N. (2021). Cancer stem cells and nucleolin as drivers of carcinogenesis. *Pharmaceuticals*, *14*(1), 1–21. https://doi.org/10.3390/PH14010060

Chen, J. Q., & Russo, J. (2009). ERα-negative and triple negative breast cancer: Molecular features and potential therapeutic approaches. *Biochimica et Biophysica Acta (BBA) - Reviews on Cancer*, *1796*(2), 162–175. https://doi.org/10.1016/J.BBCAN.2009.06.003

Cinatl, J., Wass, M. N., & Michaelis, M. (2024). Drug-resistant cell lines in cancer. *Nature Communications 2024 15:1*. https://www.nature.com/articles/s41467-024-52441-z

Cleator, S., Heller, W., & Coombes, R. C. (2007). Triple-negative breast cancer: therapeutic options. *Lancet Oncology*, *8*(3), 235–244. https://doi.org/10.1016/S1470-2045(07)70074-8/ASSET/85B6B601-916E-4E53-97D0-DA0B8821E1FF/MAIN.ASSETS/GR3.SML

Dean, M., Fojo, T., & Bates, S. (2005). Tumour stem cells and drug resistance. *Nature Reviews Cancer*, *5*(4), 275–284. https://doi.org/10.1038/NRC1590

DeVita, V. T., & Chu, E. (2008). A History of Cancer Chemotherapy. *Cancer Research*, *68*(21), 8643–8653. https://doi.org/10.1158/0008-5472.CAN-07-6611

Emadi, A., Jones, J. R., & Robert, A. B. (2009). Cyclophosphamide and cancer: golden anniversary. *Nat. Rev. Clin. Oncol*, *6*, 638–647. https://doi.org/10.1038/nrclinonc.2009.146

Evans, K. W., Yuca, E., Scott, S. S., Zhao, M., Arango, N. P., Cruz Pico, C. X., Saridogan, T., Shariati, M., Class, C. A., Bristow, C. A., Vellano, C. P., Zheng, X., Gonzalez-Angulo, A. M., Su, X., Tapia, C., Chen, K., Akcakanat, A., Lim, B., Tripathy, D., … Meric-Bernstam, F. (2021). Oxidative phosphorylation is a metabolic vulnerability in chemotherapy-resistant triple-negative breast cancer. *Cancer Research*, *81*(21), 5572–5581. https://doi.org/10.1158/0008-5472.CAN-20-3242/673639/AM/OXIDATIVE-PHOSPHORYLATION-IS-A-METABOLIC

Fasano, J., & Muggia, F. (2009). Breast cancer arising in a BRCA-mutated background: therapeutic implications from an animal model and drug development. *Annals of*

Oncology, *20*(4), 609–614. https://doi.org/10.1093/ANNONC/MDN669

Fiorillo, M., Lamb, R., Tanowitz, H. B., Mutti, L., Krstic-Demonacos, M., Cappello, A. R., Martinez-Outschoorn, U. E., Sotgia, F., & Lisanti, M. P. (2016). Repurposing atovaquone: targeting mitochondrial complex III and OXPHOS to eradicate cancer stem cells. *Oncotarget*, *7*(23), 34084–34099. https://doi.org/10.18632/ONCOTARGET.9122

Garrido-Castro, A. C., Lin, N. U., & Polyak, K. (2019). Insights into molecular classifications of triple-negative breast cancer: Improving patient selection for treatment. In *Cancer Discovery* (Vol. 9, Issue 2). https://doi.org/10.1158/2159-8290.CD-18-1177

Giroux Leprieur, E., Vieira, T., Antoine, M., Rozensztajn, N., Rabbe, N., Ruppert, A. M., Lavole, A., Cadranel, J., & Wislez, M. (2016). Sonic Hedgehog Pathway Activation Is Associated With Resistance to Platinum-Based Chemotherapy in Advanced Non–Small-Cell Lung Carcinoma. *Clinical Lung Cancer*, *17*(4), 301–308. https://doi.org/10.1016/J.CLLC.2015.12.007

Gray, M. W. (2012). Mitochondrial Evolution. *Cold Spring Harbor Perspectives in Biology*, *4*(9), a011403. https://doi.org/10.1101/CSHPERSPECT.A011403

Greaves, M., & Maley, C. C. (2012). CLONAL EVOLUTION IN CANCER. *Nature*, *481*(7381), 306. https://doi.org/10.1038/NATURE10762

Guerra, F., Arbini, A. A., & Moro, L. (2017). Mitochondria and cancer chemoresistance. *Biochimica et Biophysica Acta (BBA) - Bioenergetics*, *1858*(8), 686–699. https://doi.org/10.1016/J.BBABIO.2017.01.012

Hamed, A. R., Abdel-Azim, N. S., Shams, K. A., & Hammouda, F. M. (2019). Targeting multidrug resistance in cancer by natural chemosensitizers. *Bulletin of the National Research Centre*, *43*. https://doi.org/10.1186/s42269-019-0043-8

Han, Z., Feng, J., Hong, Z., Chen, L., Li, W., Liao, S., Wang, X., Ji, T., Wang, S., Ma, D., Chen, G., & Gao, Q. (2013). Silencing of the STAT3 signaling pathway reverses the inherent and induced chemoresistance of human ovarian cancer cells. *Biochemical and Biophysical Research Communications*, *435*(2), 188–194. https://doi.org/10.1016/J.BBRC.2013.04.087

Hanahan, D., & Weinberg, R. A. (2011a). Hallmarks of cancer: the next generation. *Cell*, *144*(5), 646–674. https://doi.org/10.1016/J.CELL.2011.02.013

Hanahan, D., & Weinberg, R. A. (2011b). Hallmarks of cancer: the next generation. *Cell*, *144*(5), 646–674. https://doi.org/10.1016/J.CELL.2011.02.013

Henkenius, K., Greene, B. H., Barckhausen, C., Hartmann, R., Märken, M., Kaiser, T., Rehberger, M., Metzelder, S. K., Parak, W. J., Neubauer, A., Brendel, C., & Mack, E. (2017). Maintenance of cellular respiration indicates drug resistance in acute myeloid leukemia. *Leukemia Research*, *62*, 56–63. https://doi.org/10.1016/J.LEUKRES.2017.09.021

Holohan, C., Van Schaeybroeck, S., Longley, D. B., & Johnston, P. G. (2013). Cancer drug resistance: an evolving paradigm. *Nature Reviews Cancer 2013 13:10*, *13*(10), 714–726. https://doi.org/10.1038/nrc3599

Housman, G., Byler, S., Heerboth, S., Lapinska, K., Longacre, M., Snyder, N., & Sarkar, S. (2014). Drug Resistance in Cancer: An Overview. *Cancers 2014, Vol. 6, Pages 1769-1792*, *6*(3), 1769–1792. https://doi.org/10.3390/CANCERS6031769

Januchowski, R., Wojtowicz, K., & Zabel, M. (2013). The role of aldehyde dehydrogenase (ALDH) in cancer drug resistance. *Biomedicine & Pharmacotherapy*, *67*(7), 669–680. https://doi.org/10.1016/J.BIOPHA.2013.04.005

Johnson, K. S., Conant, E. F., & Soo, M. S. (2021). Molecular Subtypes of Breast Cancer: A Review for Breast Radiologists. *Journal of Breast Imaging*, *3*(1), 12–24. https://doi.org/10.1093/JBI/WBAA110

Kadioglu, O., Saeed, M. E. M., Valoti, M., Frosini, M., Sgaragli, G., & Efferth, T. (2016). Interactions of human P-glycoprotein transport substrates and inhibitors at the drug binding domain: Functional and molecular docking analyses. *Biochemical Pharmacology*, *104*, 42–51. https://doi.org/10.1016/J.BCP.2016.01.014

Kaur, I., Batra, V., Kumar Reddy Bogireddy, N., Torres Landa, S. D., & Agarwal, V. (2023). Detection of organic pollutants, food additives and antibiotics using sustainable carbon dots. *Food Chemistry*, *406*, 135029. https://doi.org/10.1016/J.FOODCHEM.2022.135029

Knak, T., Abdullaziz, M. A., Höfmann, S., Alves Avelar, L. A., Klein, S., Martin, M., Fischer, M., Tanaka, N., & Kurz, T. (2022). Over 40 Years of Fosmidomycin Drug Research: A Comprehensive Review and Future Opportunities. *Pharmaceuticals (14248247)*, *15*(12), 1553. https://doi.org/10.3390/PH15121553

Koc, E. C., Burkhart, W., Blackburn, K., Moyer, M. B., Schlatzer, D. M., Moseley, A., & Spremulli, L. L. (2001). The Large Subunit of the Mammalian Mitochondrial Ribosome: ANALYSIS OF THE COMPLEMENT OF RIBOSOMAL PROTEINS PRESENT. *Journal of Biological Chemistry*, *276*(47), 43958–43969.

https://doi.org/10.1074/JBC.M106510200

Kuete, V., & Efferth, T. (2015). African Flora Has the Potential to Fight Multidrug Resistance of Cancer. *BioMed Research International*, *2015*(1), 914813. https://doi.org/10.1155/2015/914813

Kumar, A., & Jaitak, V. (2019). Natural products as multidrug resistance modulators in cancer. *European Journal of Medicinal Chemistry*, *176*, 268–291. https://doi.org/10.1016/J.EJMECH.2019.05.027

Kurebayashi, J. (2009). Possible treatment strategies for triple-negative breast cancer on the basis of molecular characteristics. *Breast Cancer*, *16*(4), 275–280. https://doi.org/10.1007/S12282-009-0111-2/TABLES/1

Kuzuyama, T., Shimizu, T., Takahashi, S., & Seto, H. (1998). Fosmidomycin, a specific inhibitor of 1-deoxy-d-xylulose 5-phosphate reductoisomerase in the nonmevalonate pathway for terpenoid biosynthesis. *Tetrahedron Letters*, *39*(43), 7913–7916. https://doi.org/10.1016/S0040-4039(98)01755-9

Lamb, R., Ozsvari, B., Lisanti, C. L., Tanowitz, H. B., Howell, A., Martinez-Outschoorn, U. E., Sotgia, F., Lisanti, M. P., Lamb, R., Ozsvari, B., Lisanti, C. L., Tanowitz, H. B., Howell, A., Martinez-Outschoorn, U. E., Sotgia, F., & Lisanti, M. P. (2015). Antibiotics that target mitochondria effectively eradicate cancer stem cells, across multiple tumor types: Treating cancer like an infectious disease. *Oncotarget*, *6*(7), 4569–4584. https://doi.org/10.18632/ONCOTARGET.3174

Lang, A., Grether-Beck, S., Singh, M., Kuck, F., Jakob, S., Kefalas, A., Altinoluk-Hambüchen, S., Graffmann, N., Schneider, M., Lindecke, A., Brenden, H., Felsner, I., Ezzahoini, H., Marini, A., Weinhold, S., Vierkötter, A., Tigges, J., Schmidt, S., Stühler, K., … Piekorz, R. P. (2016). MicroRNA-15b regulates mitochondrial ROS production and the senescence-associated secretory phenotype through sirtuin 4/SIRT4. *Aging*, *8*(3), 484–505. https://doi.org/10.18632/aging.100905

Lee, K. min, Giltnane, J. M., Balko, J. M., Schwarz, L. J., Guerrero-Zotano, A. L., Hutchinson, K. E., Nixon, M. J., Estrada, M. V., Sánchez, V., Sanders, M. E., Lee, T., Gómez, H., Lluch, A., Pérez-Fidalgo, J. A., Wolf, M. M., Andrejeva, G., Rathmell, J. C., Fesik, S. W., & Arteaga, C. L. (2017). MYC and MCL1 Cooperatively Promote Chemotherapy-Resistant Breast Cancer Stem Cells via Regulation of Mitochondrial Oxidative Phosphorylation. *Cell Metabolism*, *26*(4), 633-647.e7. https://doi.org/10.1016/J.CMET.2017.09.009

Lee, M., Hirpara, J. L., Eu, J. Q., Sethi, G., Wang, L., Goh, B. C., & Wong, A. L.

(2019). Targeting STAT3 and oxidative phosphorylation in oncogene-addicted tumors. *Redox Biology*, *25*, 101073. https://doi.org/10.1016/J.REDOX.2018.101073

Levy, J. M. M., Towers, C. G., & Thorburn, A. (2017). Targeting autophagy in cancer. *Nature Reviews Cancer 2017 17:9*, *17*(9), 528–542. https://doi.org/10.1038/nrc.2017.53

Li, S., Li, C., Ryu, H. H., Lim, S. H., Jang, W. Y., & Jung, S. (2016). Bacitracin Inhibits the Migration of U87-MG Glioma Cells via Interferences of the Integrin Outside-in Signaling Pathway. *Journal of Korean Neurosurgical Society*, *59*(2), 106. https://doi.org/10.3340/JKNS.2016.59.2.106

Lord, C. J., & Ashworth, A. (2012). The DNA damage response and cancer therapy. *Nature 2012 481:7381*, *481*(7381), 287–294. https://doi.org/10.1038/nature10760

Lytle, N. K., Barber, A. G., & Reya, T. (2018). Stem cell fate in cancer growth, progression and therapy resistance. *Nature Reviews Cancer 2018 18:11*, *18*(11), 669–680. https://doi.org/10.1038/s41568-018-0056-x

Machado, N. D., Heather, L. C., Harris, A. L., & Higgins, G. S. (2023). Targeting mitochondrial oxidative phosphorylation: lessons, advantages, and opportunities. *British Journal of Cancer 2023 129:6*, *129*(6), 897–899. https://doi.org/10.1038/s41416-023-02394-9

Margulis, L., & Bermudes, D. (1985). Symbiosis as a mechanism of evolution: status of cell symbiosis theory. *Symbiosis*, *1*, 101–124.

Massagué, J., & Obenauf, A. C. (2016). Metastatic colonization by circulating tumour cells. *Nature 2016 529:7586*, *529*(7586), 298–306. https://doi.org/10.1038/nature17038

Michael, M., & Doherty, M. M. (2005). Tumoral drug metabolism: overview and its implications for cancer therapy. *Journal of Clinical Oncology : Official Journal of the American Society of Clinical Oncology*, *23*(1), 205–229. https://doi.org/10.1200/JCO.2005.02.120

Miller, M., & Singer, M. (2022). Do antibiotics cause mitochondrial and immune cell dysfunction? A literature review. *Journal of Antimicrobial Chemotherapy*, *77*(5), 1218–1227. https://doi.org/10.1093/JAC/DKAC025

Mizushima, N., & Komatsu, M. (2011). Autophagy: Renovation of cells and tissues. *Cell*, *147*(4), 728–741. https://doi.org/10.1016/J.CELL.2011.10.026/ASSET/3DE178A3-65DE-4851-

9A94-218D77A87EEA/MAIN.ASSETS/GR4.JPG

Mostafavi, S., & Eskandari, N. (2024). Mitochondrion: Main organelle in orchestrating cancer escape from chemotherapy. *Cancer Reports*, *7*(2), e1942. https://doi.org/10.1002/CNR2.1942

Mountzios, G., Dimopoulos, M. A., & Papadimitriou, C. (2008). Excision repair cross-complementation group 1 enzyme as a molecular determinant of responsiveness to platinum-based chemotherapy for non small-cell lung cancer. *Volume 2008, Issue 3, Pages 219 - 226*, *2008*(3), 219–226. https://doi.org/10.4137/bmi.s485

Murphy, M. P., & Smith, R. A. J. (2007). Targeting antioxidants to mitochondria by conjugation to lipophilic cations. *Annual Review of Pharmacology and Toxicology*, *47*, 629–656. https://doi.org/10.1146/ANNUREV.PHARMTOX.47.120505.105110

Mustafa, S., Koran, S., & AlOmair, L. (2022). Insights Into the Role of Matrix Metalloproteinases in Cancer and its Various Therapeutic Aspects: A Review. *Frontiers in Molecular Biosciences*, *9*, 896099. https://doi.org/10.3389/FMOLB.2022.896099/BIBTEX

Napel, S., Mu, W., Jardim-Perassi, B. V., Aerts, H. J. W. L., & Gillies, R. J. (2018). Quantitative imaging of cancer in the postgenomic era: Radio(geno)mics, deep learning, and habitats. *Cancer*, *124*(24), 4633–4649. https://doi.org/10.1002/CNCR.31630

Nikolaou, M., Pavlopoulou, A., Georgakilas, A. G., & Kyrodimos, E. (2018). The challenge of drug resistance in cancer treatment: a current overview. *Clinical & Experimental Metastasis 2018 35:4*, *35*(4), 309–318. https://doi.org/10.1007/S10585-018-9903-0

O'connor, J. P. B., Rose, C. J., Waterton, J. C., Carano, R. A. D., Parker, G. J. M., & Jackson, A. (2014). *Imaging Intratumor Heterogeneity: Role in Therapy Response, Resistance, and Clinical Outcome*. https://doi.org/10.1158/1078-0432.CCR-14-0990

O'Connor, M. J. (2015). Targeting the DNA Damage Response in Cancer. *Molecular Cell*, *60*(4), 547–560. https://doi.org/10.1016/J.MOLCEL.2015.10.040

Oun, R., Moussa, Y. E., & Wheate, N. J. (2018). The side effects of platinum-based chemotherapy drugs: a review for chemists. *Dalton Transactions*, *47*(19), 6645–6653. https://doi.org/10.1039/C8DT00838H

Parkin, D. M., Bray, F., Ferlay, J., & Pisani, P. (2005). Global Cancer Statistics, 2002.

CA: A Cancer Journal for Clinicians, *55*(2), 74–108. https://doi.org/10.3322/CANJCLIN.55.2.74

Patravale, V., Dandekar, P., & Jain, R. (2012). Nanotoxicology: evaluating toxicity potential of drug-nanoparticles. *Nanoparticulate Drug Delivery*, 123–155. https://doi.org/10.1533/9781908818195.123

Perez, E. A. (2004). Carboplatin in Combination Therapy for Metastatic Breast Cancer. *The Oncologist*, *9*(5). https://doi.org/10.1634/theoncologist.9-5-518

Peters, G. J., Backus, H. H. J., Freemantle, S., Van Triest, B., Codacci-Pisanelli, G., Van der Wilt, C. L., Smid, K., Lunec, J., Calvert, A. H., Marsh, S., McLeod, H. L., Bloemena, E., Meijer, S., Jansen, G., Van Groeningen, C. J., & Pinedo, H. M. (2002). Induction of thymidylate synthase as a 5-fluorouracil resistance mechanism. *Biochimica et Biophysica Acta (BBA) - Molecular Basis of Disease*, *1587*(2–3), 194–205. https://doi.org/10.1016/S0925-4439(02)00082-0

Pinto, C. A., Widodo, E., Waltham, M., & Thompson, E. W. (2013). Breast cancer stem cells and epithelial mesenchymal plasticity - Implications for chemoresistance. *Cancer Letters*, *341*(1), 56–62. https://doi.org/10.1016/J.CANLET.2013.06.003

Plaks, V., Kong, N., & Werb, Z. (2015). The Cancer Stem Cell Niche: How Essential Is the Niche in Regulating Stemness of Tumor Cells? *Cell Stem Cell*, *16*(3), 225–238. https://doi.org/10.1016/J.STEM.2015.02.015

Ramos, A., Sadeghi, S., & Tabatabaeian, H. (2021). Battling Chemoresistance in Cancer: Root Causes and Strategies to Uproot Them. *International Journal of Molecular Sciences 2021, Vol. 22, Page 9451*, *22*(17), 9451. https://doi.org/10.3390/IJMS22179451

Rayner, D. M., & Cutts, S. M. (2023). Anthracyclines. *Side Effects of Drugs Annual*, *36*, 683–694. https://doi.org/10.1016/B978-0-444-63407-8.00045-9

Ribatti, D., Tamma, R., & Annese, T. (2020). Epithelial-Mesenchymal Transition in Cancer: A Historical Overview. *Translational Oncology*, *13*(6), 100773. https://doi.org/10.1016/J.TRANON.2020.100773

Samuel, S. M., Varghese, E., Koklesová, L., Líšková, A., Kubatka, P., & Büsselberg, D. (2020). Counteracting Chemoresistance with Metformin in Breast Cancers: Targeting Cancer Stem Cells. *Cancers 2020, Vol. 12, Page 2482*, *12*(9), 2482. https://doi.org/10.3390/CANCERS12092482

Sandoval-Acuña, C., Fuentes-Retamal, S., Guzmán-Rivera, D., Peredo-Silva, L., Madrid-Rojas, M., Rebolledo, S., Castro-Castillo, V., Pavani, M., Catalán, M.,

Maya, J. D., Jara, J. A., Parra, E., Calaf, G. M., Speisky, H., & Ferreira, J. (2016). Destabilization of mitochondrial functions as a target against breast cancer progression: Role of TPP+-linked-polyhydroxybenzoates. *Toxicology and Applied Pharmacology*, *309*, 2–14. https://doi.org/10.1016/J.TAAP.2016.08.018

Shao, Y., Li, X., Wood, J. W., & Ma, J. xing. (2018). Mitochondrial dysfunctions, endothelial progenitor cells and diabetic retinopathy. *Journal of Diabetes and Its Complications*, *32*(10), 966–973. https://doi.org/10.1016/j.jdiacomp.2018.06.015

Sharma, P., Hu-Lieskovan, S., Wargo, J. A., & Ribas, A. (2017). Primary, Adaptive, and Acquired Resistance to Cancer Immunotherapy. *Cell*, *168*(4), 707–723. https://doi.org/10.1016/J.CELL.2017.01.017

Sivandzade, F., Bhalerao, A., & Cucullo, L. (2019). Analysis of the Mitochondrial Membrane Potential Using the Cationic JC-1 Dye as a Sensitive Fluorescent Probe. *Bio-Protocol*, *9*(1), e3128–e3128. https://doi.org/10.21769/BIOPROTOC.3128

Škrtić, M., Sriskanthadevan, S., Jhas, B., Gebbia, M., Wang, X., Wang, Z., Hurren, R., Jitkova, Y., Gronda, M., Maclean, N., Lai, C. K., Eberhard, Y., Bartoszko, J., Spagnuolo, P., Rutledge, A. C., Datti, A., Ketela, T., Moffat, J., Robinson, B. H., … Schimmer, A. D. (2011). Inhibition of Mitochondrial Translation as a Therapeutic Strategy for Human Acute Myeloid Leukemia. *Cancer Cell*, *20*(5), 674–688. https://doi.org/10.1016/J.CCR.2011.10.015

Sládek, N. E., Kollander, R., Sreerama, L., & Kiang, D. T. (2002). Cellular levels of aldehyde dehydrogenases (ALDH1A1 and ALDH3A1) as predictors of therapeutic responses to cyclophosphamide-based chemotherapy of breast cancer: a retrospective study. Rational individualization of oxazaphosphorine-based cancer chemotherapeutic regimens. *Cancer Chemotherapy and Pharmacology*, *49*(4), 309–321. https://doi.org/10.1007/S00280-001-0412-4

Sørlie, T., Perou, C. M., Tibshirani, R., Aas, T., Geisler, S., Johnsen, H., Hastie, T., Eisen, M. B., Van De Rijn, M., Jeffrey, S. S., Thorsen, T., Quist, H., Matese, J. C., Brown, P. O., Botstein, D., Lønning, P. E., & Børresen-Dale, A. L. (2001). Gene expression patterns of breast carcinomas distinguish tumor subclasses with clinical implications. *Volume 98, Issue 19, Pages 10869 - 10874*, *98*(19), 10869–10874. https://doi.org/10.1073/pnas.191367098

Sosa, M. S., Bragado, P., & Aguirre-Ghiso, J. A. (2014). Mechanisms of disseminated cancer cell dormancy: an awakening field. *Nature Reviews Cancer 2014 14:9*, *14*(9), 611–622. https://doi.org/10.1038/nrc3793

Steeg, P. S. (2006). Tumor metastasis: mechanistic insights and clinical challenges. *Nature Medicine 2006 12:8*, *12*(8), 895–904. https://doi.org/10.1038/nm1469

Stork, C. M., & Schreffler, S. M. (2014). Cyclophosphamide. *Encyclopedia of Toxicology: Third Edition*, 1111–1113. https://doi.org/10.1016/B978-0-12-386454-3.00720-X

Sun, W. L., Chen, J., Wang, Y. P., & Zheng, H. (2011). Autophagy protects breast cancer cells from epirubicin-induced apoptosis and facilitates epirubicin-resistance development. *Autophagy*, *7*(9), 1035–1044. https://doi.org/10.4161/AUTO.7.9.16521

Takeuchi, K., Motoda, Y. I., & Ito, F. (2006). Role of transcription factor activator protein 1 (AP1) in epidermal growth factor-mediated protection against apoptosis induced by a DNA-damaging agent. *The FEBS Journal*, *273*(16), 3743–3755. https://doi.org/10.1111/J.1742-4658.2006.05377.X

Tham, M., & Abastado, J. P. (2011). Escape of tumor immune surveillance and metastasis. *Drug Discovery Today: Disease Models*, *8*(2–3), 81–86. https://doi.org/10.1016/J.DDMOD.2011.07.004

Tsou, S. H., Chen, T. M., Hsiao, H. T., & Chen, Y. H. (2015). A critical dose of doxorubicin is required to alter the gene expression profiles in MCF-7 cells acquiring multidrug resistance. *PLoS ONE*, *10*(1). https://doi.org/10.1371/JOURNAL.PONE.0116747

Uslu, C., Kapan, E., & Lyakhovich, A. (2024). Cancer resistance and metastasis are maintained through oxidative phosphorylation. *Cancer Letters*, *587*. https://doi.org/10.1016/J.CANLET.2024.216705

Vamvakas, A., Vassiou, K., Tsivaka, D., & Tsougos, I. (2020). Decision support systems in breast cancer. *Precision Medicine for Investigators, Practitioners and Providers*, 319–327. https://doi.org/10.1016/B978-0-12-819178-1.00031-9

Vardanyan, R. S., & Hruby, V. J. (2006). Antibiotics. *Synthesis of Essential Drugs*, 425–498. https://doi.org/10.1016/B978-044452166-8/50032-7

Vasan, K., Werner, M., & Chandel, N. S. (2020). Mitochondrial Metabolism as a Target for Cancer Therapy. *Cell Metabolism*, *32*(3), 341–352. https://doi.org/10.1016/J.CMET.2020.06.019

Viale, A., Pettazzoni, P., Lyssiotis, C. A., Ying, H., Sánchez, N., Marchesini, M., Carugo, A., Green, T., Seth, S., Giuliani, V., Kost-Alimova, M., Muller, F., Colla, S., Nezi, L., Genovese, G., Deem, A. K., Kapoor, A., Yao, W., Brunetto, E., …

Draetta, G. F. (2014). Oncogene ablation-resistant pancreatic cancer cells depend on mitochondrial function. *Nature*, *514*(7524), 628–632. https://doi.org/10.1038/NATURE13611

Vyas, S., Zaganjor, E., & Haigis, M. C. (2016). Mitochondria and Cancer. *Cell*, *166*(3), 555–566. https://doi.org/10.1016/J.CELL.2016.07.002

Waks, A. G., & Winer, E. P. (2019). Breast Cancer Treatment. *JAMA*, *321*(3), 316–316. https://doi.org/10.1001/JAMA.2018.20751

Wang, F., Ma, L., Zhang, Z., Liu, X., Gao, H., Zhuang, Y., Yang, P., Kornmann, M., Tian, X., & Yang, Y. (2016). Hedgehog Signaling Regulates Epithelial-Mesenchymal Transition in Pancreatic Cancer Stem-Like Cells. *Journal of Cancer*, *7*(4), 408–417. https://doi.org/10.7150/JCA.13305

Wang, H., Zhang, F., Wen, H., Shi, W., Huang, Q., Huang, Y., Xie, J., Li, P., Chen, J., Qin, L., & Zhou, Y. (2020). Tumor- And mitochondria-targeted nanoparticles eradicate drug resistant lung cancer through mitochondrial pathway of apoptosis. *Journal of Nanobiotechnology*, *18*(1). https://doi.org/10.1186/S12951-019-0562-3

Warburg, O. (1956). On the origin of cancer cells. *Science (New York, N.Y.)*, *123*(3191), 309–314. https://doi.org/10.1126/SCIENCE.123.3191.309

White, E. (2012). Deconvoluting the context-dependent role for autophagy in cancer. *Nature Reviews Cancer 2012 12:6*, *12*(6), 401–410. https://doi.org/10.1038/nrc3262

Wu, C., Zhao, A., Tan, T., Wang, Y., & Shen, Z. (2019). Overexpression of microRNA-620 facilitates the resistance of triple negative breast cancer cells to gemcitabine treatment by targeting DCTD. *Experimental and Therapeutic Medicine*. https://doi.org/10.3892/ETM.2019.7601

Yang, Q., Huang, J., Wu, Q., Cai, Y., Zhu, L., Lu, X., Chen, S., Chen, C., & Wang, Z. (2014). Acquisition of epithelial-mesenchymal transition is associated with Skp2 expression in paclitaxel-resistant breast cancer cells. *British Journal of Cancer*, *110*(8), 1958–1967. https://doi.org/10.1038/BJC.2014.136

Ye, X., & Weinberg, R. A. (2015). Epithelial–Mesenchymal Plasticity: A Central Regulator of Cancer Progression. *Trends in Cell Biology*, *25*(11), 675–686. https://doi.org/10.1016/J.TCB.2015.07.012

Yeh, C. T., Su, C. L., Huang, C. Y. F., Lin, J. K. Y., Lee, W. H., Chang, P. M. H., Kuo, Y. L., Liu, Y. W., Wang, L. S., Wu, C. H., Shieh, Y. S., Jan, Y. H., Chuang, Y. J., Hsiao, M., & Wu, A. T. H. (2013). A Preclinical Evaluation of Antimycin A as a

Potential Antilung Cancer Stem Cell Agent. *Evidence-Based Complementary and Alternative Medicine*, *2013*(1), 910451. https://doi.org/10.1155/2013/910451

Zhang, J., Tian, Q., Chan, S. Y., Duan, W., & Zhou, S. (2005). Insights into oxazaphosphorine resistance and possible approaches to its circumvention. *Drug Resistance Updates*, *8*(5), 271–297. https://doi.org/10.1016/J.DRUP.2005.08.003

Zhang, P., Brinton, L. T., Gharghabi, M., Sher, S., Williams, K., Cannon, M., Walker, J. S., Canfield, D., Beaver, L., Cempre, C. B., Phillips, H., Chen, X., Yan, P., Lehman, A., Scherle, P., Wang, M., Vaddi, K., Baiocchi, R., Wang, R., … Lapalombella, R. (2022). Targeting OXPHOS de novo purine synthesis as the nexus of FLT3 inhibitor–mediated synergistic antileukemic actions. *Science Advances*, *8*(37), eabp9005. https://doi.org/10.1126/SCIADV.ABP9005

Zhang, X., Powell, K., & Li, L. (2020). Breast Cancer Stem Cells: Biomarkers, Identification and Isolation Methods, Regulating Mechanisms, Cellular Origin, and Beyond. *Cancers*, *12*(12), 1–28. https://doi.org/10.3390/CANCERS12123765

Zhao, J. (2016). Cancer stem cells and chemoresistance: The smartest survives the raid. *Pharmacology & Therapeutics*, *160*, 145–158. https://doi.org/10.1016/J.PHARMTHERA.2016.02.008

Zhao, Z., Mei, Y., Wang, Z., & He, W. (2023). The Effect of Oxidative Phosphorylation on Cancer Drug Resistance. *Cancers*, *15*(1). https://doi.org/10.3390/CANCERS15010062

Zheng, X., Carstens, J. L., Kim, J., Scheible, M., Kaye, J., Sugimoto, H., Wu, C. C., Lebleu, V. S., & Kalluri, R. (2015). Epithelial-to-mesenchymal transition is dispensable for metastasis but induces chemoresistance in pancreatic cancer. *Nature 2015 527:7579*, *527*(7579), 525–530. https://doi.org/10.1038/nature16064

Zong, W. X., Rabinowitz, J. D., & White, E. (2016). Mitochondria and Cancer. *Molecular Cell*, *61*(5), 667–676. https://doi.org/10.1016/J.MOLCEL.2016.02.011